Clinical and Translational Report

Cell Metabolism

A Periodic Diet that Mimics Fasting Promotes Multi-System Regeneration, Enhanced Cognitive Performance, and Healthspan

Graphical Abstract

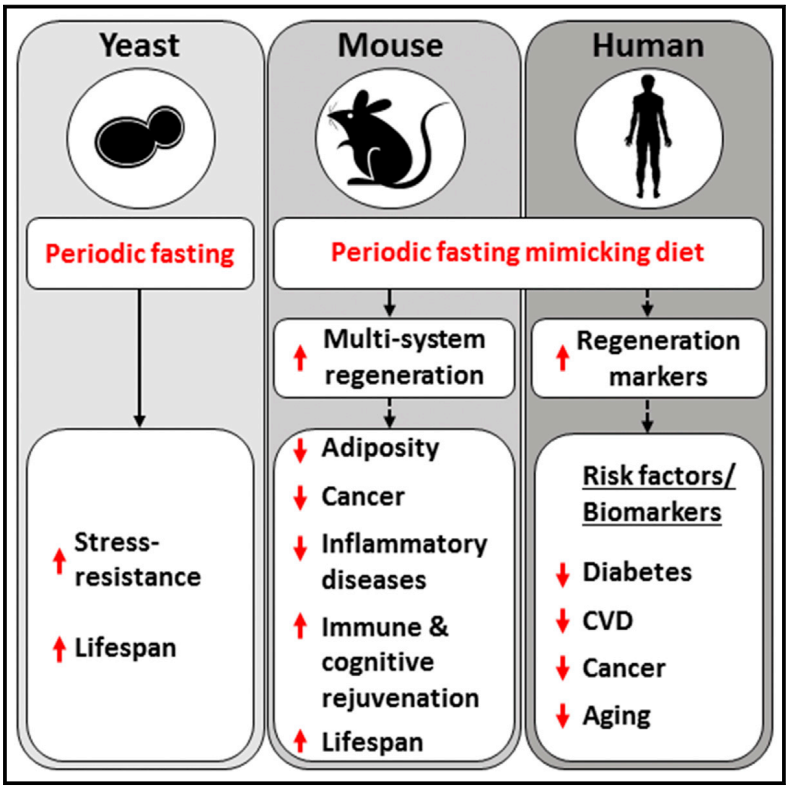

Highlights

- FMD rejuvenates the immune system and reduces cancer incidence in C57BL/6 mice
- FMD promotes hippocampal neurogenesis and improves cognitive performance in mice
- FMD causes beneficial changes in risk factors of age-related diseases in humans

Authors

Sebastian Brandhorst, In Young Choi, Min Wei, ..., Todd E. Morgan, Tanya B. Dorff, Valter D. Longo

Correspondence

vlongo@usc.edu

In Brief

Brandhorst et al. develop a fasting mimicking diet (FMD) protocol, which retains the health benefits of prolonged fasting. In mice, FMD improved metabolism and cognitive function, decreased bone loss and cancer incidence, and extended longevity. In humans, three monthly cycles of a 5-day FMD reduced multiple risk factors of aging

Brandhorst et al., 2015, Cell Metabolism *22*, 86–99
July 7, 2015
http://dx.doi.org/10.1016/j.cmet.2015.05.012

CellPress

CellPress

Cell Metabolism
Clinical and Translational Report

A Periodic Diet that Mimics Fasting Promotes Multi-System Regeneration, Enhanced Cognitive Performance, and Healthspan

Sebastian Brandhorst,[1,15] In Young Choi,[1,15] Min Wei,[1] Chia Wei Cheng,[1] Sargis Sedrakyan,[2] Gerardo Navarrete,[1] Louis Dubeau,[3] Li Peng Yap,[4] Ryan Park,[4] Manlio Vinciguerra,[5] Stefano Di Biase,[1] Hamed Mirzaei,[1] Mario G. Mirisola,[6] Patra Childress,[7] Lingyun Ji,[8] Susan Groshen,[8] Fabio Penna,[9] Patrizio Odetti,[10] Laura Perin,[2] Peter S. Conti,[4] Yuji Ikeno,[11] Brian K. Kennedy,[12] Pinchas Cohen,[1] Todd E. Morgan,[1] Tanya B. Dorff,[13] and Valter D. Longo[1,14,*]

[1]Longevity Institute, School of Gerontology, and Department of Biological Sciences, University of Southern California, Los Angeles, CA 90089, USA
[2]GOFARR Laboratory, Children's Hospital Los Angeles, Division of Urology, Saban Research Institute, University of Southern California, Los Angeles, CA 90089, USA
[3]Department of Pathology, Keck School of Medicine, University of Southern California, Los Angeles, CA 90089, USA
[4]Molecular Imaging Center, Department of Radiology, Keck School of Medicine, University of Southern California, Los Angeles, CA 90089, USA
[5]Institute for Liver and Digestive Health, Division of Medicine, University College London, Royal Free Hospital, London NW3 2PF, UK
[6]Department of Pathobiology and Medical Biotechnology, University of Palermo, 90100 Palermo, Italy
[7]Global Medicine Program, Keck School of Medicine, University of Southern California, Los Angeles, CA 90089, USA
[8]Department of Preventive Medicine, Keck School of Medicine, University of Southern California, Los Angeles, CA 90089, USA
[9]Department of Clinical and Biological Sciences, University of Torino, 10100 Torino, Italy
[10]Department of Internal Medicine, University of Genova, 16146 Genova, Italy
[11]Department of Pathology, Barshop Institute, University of Texas Health Science Center, San Antonio, TX 78229, USA
[12]Buck Institute for Research on Aging, Novato, CA 94945, USA
[13]Norris Comprehensive Cancer Center, Keck School of Medicine, University of Southern California, Los Angeles, CA 90089, USA
[14]IFOM, FIRC Institute of Molecular Oncology, 20139 Milano, Italy
[15]Co-first author
*Correspondence: vlongo@usc.edu
http://dx.doi.org/10.1016/j.cmet.2015.05.012

SUMMARY

Prolonged fasting (PF) promotes stress resistance, but its effects on longevity are poorly understood. We show that alternating PF and nutrient-rich medium extended yeast lifespan independently of established pro-longevity genes. In mice, 4 days of a diet that mimics fasting (FMD), developed to minimize the burden of PF, decreased the size of multiple organs/systems, an effect followed upon re-feeding by an elevated number of progenitor and stem cells and regeneration. Bi-monthly FMD cycles started at middle age extended longevity, lowered visceral fat, reduced cancer incidence and skin lesions, rejuvenated the immune system, and retarded bone mineral density loss. In old mice, FMD cycles promoted hippocampal neurogenesis, lowered IGF-1 levels and PKA activity, elevated NeuroD1, and improved cognitive performance. In a pilot clinical trial, three FMD cycles decreased risk factors/biomarkers for aging, diabetes, cardiovascular disease, and cancer without major adverse effects, providing support for the use of FMDs to promote healthspan.

INTRODUCTION

Dietary composition and calorie level are key factors affecting aging and age-related diseases (Antosh et al., 2011; Blagosklonny et al., 2009; Fontana et al., 2010; Gems and Partridge, 2013; López-Otín et al., 2013; Tatar et al., 2003). Dietary restriction (DR) promotes metabolic and cellular changes that affect oxidative damage and inflammation, optimize energy metabolism, and enhance cellular protection (Haigis and Yankner, 2010; Johnson et al., 2000; Lee et al., 2012b; Longo and Finch, 2003; Mair and Dillin, 2008; Narasimhan et al., 2009; Smith et al., 2008). Fasting, the most extreme form of DR, which entails the abstinence from all food, but not water, can be applied in a chronic manner as intermittent fasting (IF) or periodically as cycles of prolonged fasting (PF) lasting 2 or more days (Longo and Mattson, 2014). In rodents, IF promotes protection against diabetes, cancer, heart disease, and neuro-degeneration (Longo and Mattson, 2014). In humans, IF and less-severe regimens (e.g., consumption of approximately 500 kcal/day for 2 days a week) have beneficial effects on insulin, glucose, C-reactive protein, and blood pressure (Harvie et al., 2011).

PF cycles lasting 2 or more days, but separated by at least a week of a normal diet, are emerging as a highly effective strategy to protect normal cells and organs from a variety of toxins and toxic conditions (Raffaghello et al., 2008; Verweij et al., 2011) while increasing the death of many cancer cell types (Lee et al., 2012a; Shi et al., 2012). PF causes a decrease in blood glucose,

insulin, and insulin-like growth factor 1 (IGF-1) (Lee et al., 2010) and is accompanied by autophagy (Cuervo et al., 2005; Madeo et al., 2010). Recently, we have shown that PF causes a major reduction in the levels of white blood cells followed by stem-cell-based immune system regeneration upon refeeding (Cheng et al., 2014). Others have reported on the role of PF in causing major decreases in liver and body mass in rats (Wasselin et al., 2014). However, prolonged water-only fasting is difficult for the great majority of the population, and its extreme nature could cause adverse effects, which include the exacerbation of previous malnourishments and dysfunctions, particularly in old and frail subjects. These concerns point to the need for dietary interventions that induce PF-like effects while minimizing the risk of adverse effects and the burden of complete food restriction.

Here we identified a diet that mimics the effects of fasting (fasting mimicking diet, FMD) on markers associated with the stress resistance caused by PF, including low levels of glucose and IGF-1 and high levels of ketone bodies and IGFBP-1 (Longo and Mattson, 2014). We tested the hypothesis that cycles of the FMD lasting 4 days followed by a standard ad libitum diet could promote healthspan in mice. Additionally, we tested the effects of three cycles of a similar FMD in a pilot randomized clinical study with 38 subjects, 19 of whom were assigned to the FMD group.

RESULTS AND DISCUSSION

Periodic Fasting in *S. cerevisiae* Extends Lifespan and Induces Stress Resistance

To determine whether the benefits of periodic starvation can be achieved in a simple organism, we tested the effects of cycles of prolonged fasting (PF) in *S. cerevisiae.* PF was implemented by switching wild-type yeast cells back and forth from nutrient-rich medium to water every 48 hr. This duration was selected to match the length of fasting shown to be effective in mice, but also to allow cells to undergo at least 4 cycles of PF within its lifespan. PF cycles extended both medium and maximum chronological lifespan (Figures 1A and 1B) and increased the number of yeast cells that survive hydrogen peroxide treatment by more than 100-fold (Figure 1C). Surprisingly, the deletion of the serine threonine kinase Rim15, or of its downstream stress response transcription factors Msn2/4 and Gis1, well established to be important or essential for longevity extension by genetic and dietary interventions (Fabrizio et al., 2001; Wei et al., 2008), did not prevent the lifespan effects of PF (Figures 1A and 1B). These results indicate that PF can protect simple organisms from both toxins and aging by mechanisms that are in part independent of conserved pro-longevity transcription factors, in agreement with findings in *C. elegans* that complete deprivation of food does not require the stress response transcription factor DAF-16, analogue of yeast Msn2/4 and Gis1 (Greer and Brunet, 2009; Kaeberlein et al., 2006).

Periodic FMD in Aged Mice

Periodic FMD without an Overall Reduction in Calorie Intake Promotes Visceral Fat Loss

We developed a very low calorie/low protein fasting mimicking diet (FMD) that causes changes in markers associated with stress resistance or longevity (IGF-1, IGFBP-1, ketone bodies, and glucose) that are similar to those caused by fasting (Table S1). Mice were fed the FMD starting at 16 months of age for 4 days twice a month and were fed an ad libitum diet in the period between FMD cycles. Mice on the control diet reached maximum weight (36.6 ± 5.2 g) at 21.5 months of age, whereas those in the FMD group lost ~15% weight during each FMD cycle but re-gained most of the weight upon re-feeding (Figure S1A). However, FMD group mice maintained a constant weight between 16 and 22 months and then gradually lost weight (Figure 1D). Although FMD group mice were severely calorically restricted during the diet, they compensated for this restriction by over-eating during the ad libitum period, resulting in a 14-day cumulative calorie intake equivalent to that of the ad libitum groups (Figures 1E and S1B). The average caloric intake in both cohorts increased after 25 months of age (Figure 1E).

At the end of the FMD and before re-feeding, blood glucose levels were 40% lower than those in the control diet group. Throughout the study, glucose returned to normal levels within 7 days of re-feeding (Figure S1C). Ketone bodies increased ~9-fold by the end of the FMD but returned to normal levels after re-feeding (Figure S1D). Serum insulin levels were reduced 10-fold after 4 days of the FMD and returned to baseline levels after re-feeding (Figure S1E). Reduced signaling of the growth hormone/IGF-1 axis extends health- and lifespan in rodents (Brown-Borg, 2009; Guarente and Kenyon, 2000; Harrison et al., 2009; Junnila et al., 2013; Wullschleger et al., 2006). IGF-1 was reduced by ~45% by the end of the FMD period but returned to normal levels, even after multiple FMD cycles (Figure S1F). IGFBP-1, which inhibits IGF-1, increased 8-fold by the end of the FMD regimen, but its concentration returned to levels similar to those for ad libitum mice within 1 week of re-feeding (Figure S1G).

To investigate diet-induced body composition changes, we evaluated lean body mass and body fat localization by microCT. At 28 months, FMD group mice showed a trend ($p = 0.06$) for reduced total adipose tissue measured during the ad libitum diet period between cycles (Figure 1F). Although subcutaneous adipose tissue volume (Figures 1G, 1J, and 1K; gray area) was not affected, visceral fat deposits (Figures 1H, 1J, and 1K; red area) were reduced in the FMD group compared to control group mice ($p < 0.05$). Lean body mass remained similar in the two groups (Figure 1I). These results indicate that FMD cycles can have profound effects on visceral fat, glucose, and IGF-1 levels, but in mice the latter changes are reversed by the return to the ad libitum diet.

Reduced Organ Size and Regeneration

FMD (20.5 months), FMD-RF (7 days after resuming the ad libitum diet post-FMD; 20.5 months), and ad libitum-fed (16 and 20.5 months) mice were euthanized, and organ weights were measured. At the end of the FMD, we observed a reduction in organ weight in kidneys, heart, and liver (Figures 1L–1N), but not in the lungs, spleen, and brain (Figures S1L and S1M), and a reduction in body weight (Figure S1H–S1J). The weights of these organs returned to pre-FMD levels after re-feeding.

The chronic use of bi-weekly FMD cycles caused no differences in systolic and diastolic left ventricular volume, ejection fraction, and left ventricular mass, as measures of cardiac function in 25-month-old mice (Figures S1N–S1Q). Serum alanine transaminase, a liver atrophy marker, increased at the end of the FMD but returned to control levels upon re-feeding

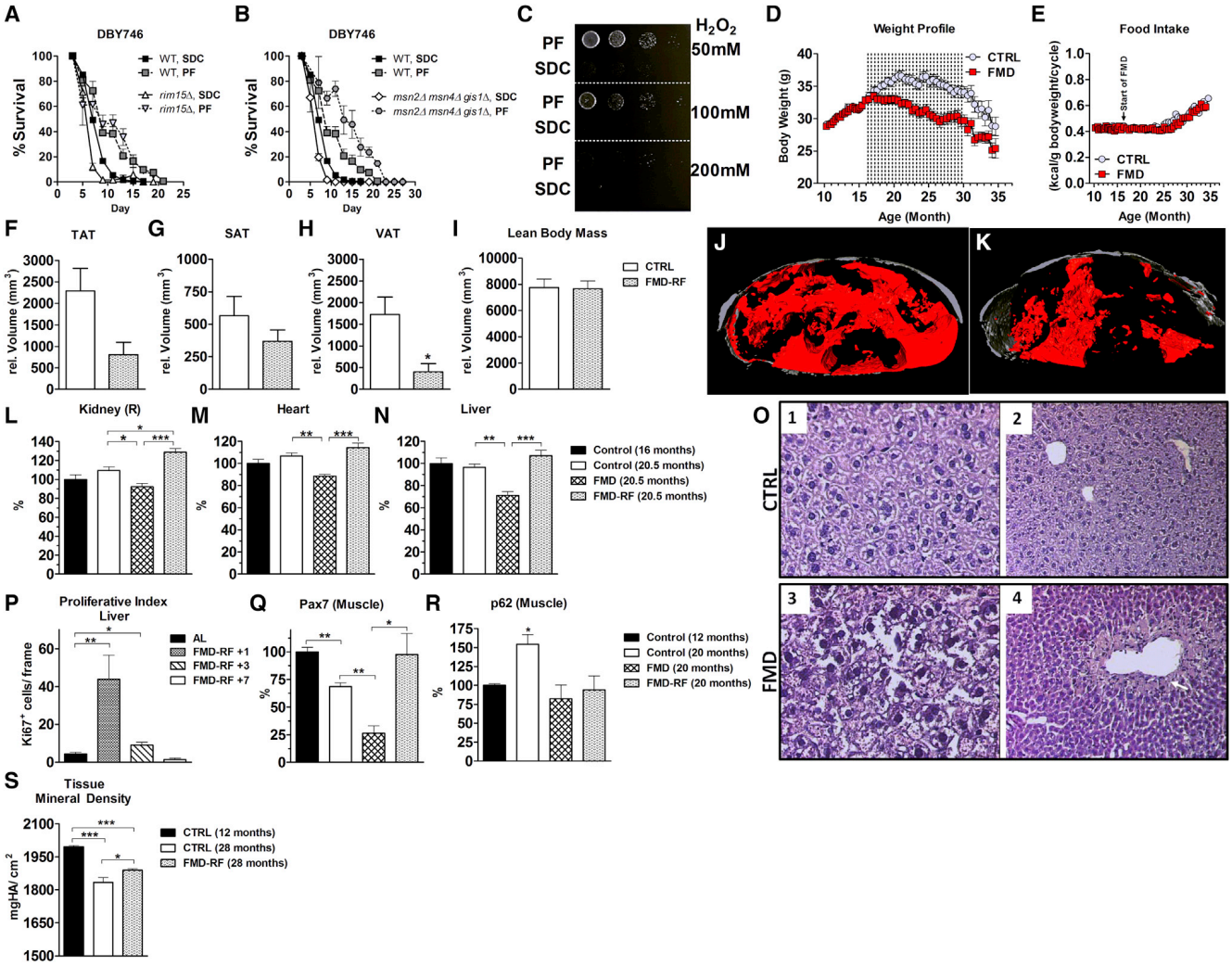

Figure 1. Periodic FMD Promotes a Lean Bodyweight, Improves Healthspan, and Promotes Tissue Regeneration

(A and B) Periodic fasting (PF, alternating cycles of SDC media and water) prolongs lifespan in wild-type (WT) *S. cerevisiae* (DBY746) and *rim15*Δ (A) and *msn2*Δ *msn4*Δ *gis1*Δ DBY746 (B) mutants.

(C) PF induces cellular stress resistance against hydrogen peroxide in *S. cerevisiae* (DBY746).

(D) Mouse body weight profile. Dotted lines represent FMD cycles.

(E) Consumed kcal/g of bodyweight.

(F–I) Total adipose tissue (TAT) (F), subcutaneous adipose tissue (SAT) (G), visceral adipose tissue (VAT) (H), and lean body mass (I) at 28 months of age. n = 3/group.

(J and K) Representative images of the SAT (gray) (J) and VAT (red) (K) in the lumbar L3 region.

(L–N) Kidney (L), heart (M), and liver (N) weight as percentage change. n = 8–10/group.

(O) Liver H&E staining of control (1, 2) and FMD mouse at the end of the FMD regimen (3) or 24 hr after re-feeding (4). Unorganized cells (arrow) indicate liver repopulation. 1, 3: 40× magnification; 2, 4: 20× magnification.

(P) Hepatic proliferative index ($Ki67^+$) after 1, 3, and 7 days of refeeding compared to control. n = 3–4/group.

(Q and R) Pax7 (Q) and p62 (R) protein expression level. n = 3–4/group.

(S) Tissue mineral density (mg Hydroxyapatite/cm^3) of the femur. n = 5/group.

All data are expressed as the mean ± SEM.

(Figure S1R). Following re-feeding, liver cells repopulated in proximity to the hepatic blood vessels (Figure 1O 4, arrow). The effect of the FMD on hepatic regeneration 24 hr post re-feeding was supported by a 10-fold induction of a marker for hepatic cellular proliferation (Ki67), which is absent in G_0 cells (Figures 1P and S1S). Ki67 remained elevated for at least 3 days post-FMD. Renal function, assessed by serum creatinine and blood urea nitrogen measurements, revealed no alterations (Figures S1T and S1U) (Schnell et al., 2002). Renal histology, to evaluate glomerular and interstitial fibrosis, also showed no change in the number of sclerotic glomeruli (Figure S1V). These data are supportive of hepatic regeneration as a consequence of FMD-re-feeding cycles and with the absence either liver or kidney toxicity even after 4 months on the FMD.

Postnatal growth and regeneration of the skeletal muscle requires myogenic precursors termed satellite cells (Sinha et al., 2014). Pax7 expression is critical for satellite cell biogenesis, survival, and self-renewal (Olguin et al., 2007), whereas the myogenic transcription factors MyoD and MyoG promote muscle development and differentiation (Perry and Rudnick, 2000). Pax7 upregulation and reduced MyoD expression is observed in undifferentiated myogenic cells (Olguin et al., 2007). An age-dependent decline in Pax7 (Figure 1Q) and MyoD (and less pronounced in MyoG) was detected in 20-month-old mice (Figures S1W and S1X). At the end of the FMD, Pax7 expression was reduced by ~40% compared to that in control animals. A similar trend was also observed for MyoG ($p = 0.074$). 1 week after refeeding, Pax7 expression in 20-month-old FMD group animals reached levels similar to those in 12-month-old ad libitum fed animals (Figure 1Q). By contrast, MyoD expression in old animals was not altered by the FMD (Figures S1W and S1X). Taken together, these changes are consistent with muscle regeneration and rejuvenation upon re-feeding, although further analyses similar to those performed for the hematopoietic and nervous systems (see below) are necessary to confirm this hypothesis and determine the mechanisms responsible for it. Heterochronic parabiosis has been shown to increase the proliferative index of aged hepatocytes, as well as the proliferative and regenerative capacity of aged muscle satellite cells, and to promote adult neurogenesis in an age-dependent fashion in mice (Conboy and Rando, 2012; Villeda et al., 2011). One of the proteins that has been implicated in muscle and brain regeneration, and which may contribute to regenerative effects in multiple systems, is GDF11 (Katsimpardi et al., 2014; Sinha et al., 2014). It will be interesting to determine if part of the rejuvenating effect of the FMD may involve factors including or related to GDF11.

The failure to induce autophagy contributes to cellular damage, carcinogenesis, and aging (Cuervo et al., 2005). Autophagy can be monitored by indirectly measuring autophagic sequestration (LC3) and degradation (p62) (Moscat and Diaz-Meco, 2011) (Figure S1Y and S1Z). p62 is consistently increased in autophagy-deficient cells (Komatsu et al., 2007). An age-dependent increase in muscle p62 was observed in 20-month-old mice from the ad libitum, but not FMD, group (Figure 1R), indicating that the FMD and possibly the associated regeneration protects muscle cells from age-dependent functional decline, including the ability to maintain normal expression of autophagy proteins.

Tissue mineral density in both femora decreased in 28-month-old C57BL/6 mice compared to that in 12-month-old mice (Figure 1S), in agreement with previously published data (Shen et al., 2011). At 28 months, femoral bone density was higher in the FMD group compared to that in the control diet group (Figure 1S), indicating that FMD cycles either attenuated age-dependent bone mineral density loss or induced bone regeneration.

Cancer and Inflammation

C57BL/6 mice are prone to hematopoietic tumors and mainly malignant lymphomas (Blackwell et al., 1995). Subcutaneous and internal masses caused by neoplasia, abscesses, or both were detected in aging mice (Figures 2A–2H and S2A–S2D). Necropsies indicated a 45% reduction in neoplasia incidence in the FMD group compared to that in the control group (Figure 2I). By the end of life, lymphomas affected ~67% of control mice, but only ~40% of mice in the FMD group (Figure 2J), although the FMD did not cause a shift in the type of neoplasms. Notably, the FMD also postponed the occurrence of neoplasm-related deaths by over 3 months, from 25.3 ± 0.66 months in the controls to 28.8 ± 0.72 months of age in the FMD cohort ($p = 0.003$) (Figure 2K). Furthermore, necropsies revealed that the number of animals with multiple (3 or more) abnormal lesions was more than 3-fold higher in the control than in the FMD group ($p = 0.0067$; Fisher's exact test) (Figure 2L). Therefore, the cycles of the FMD started at middle age reduced tumor incidence, delayed their onset, and caused a major reduction in the number of lesions, which may reflect a general switch from malignant to benign tumors.

Inflammation can play a key role in the development of many age-related diseases including cancer (Bartke et al., 2013; Morgan et al., 2007). Pathological analysis showed a reduced number of tissues with inflammation (e.g., reactive lymph nodes or chronic hepatic inflammation, Table S2) in the FMD mice compared to those in the control group (Figure 2M). One of the inflammatory conditions observed in C57BL/6 mice is severe ulcerating dermatitis (Figure 2N). Control animals had an ~20% incidence of progressing skin lesions that required animal sacrifice in contrast to the ~10% incidence for mice in the FMD-fed group. These results indicate that the FMD protects against inflammation and inflammation-associated skin lesions (Coppé et al., 2010).

Effects of the FMD on Immunosenescence and Bone-Marrow-Derived Stem and Progenitor Cells

The age-associated decline in hematopoiesis causes a diminished or altered production of adaptive immune cells, a phenomenon known as "immunosenescence," manifested as a shift in the lymphoid-to-myeloid ratio and elevated incidence of anemia and myeloid malignancies (Figures 2O–2S) (Muller-Sieburg et al., 2004; Shaw et al., 2010). Complete blood counts indicated that the FMD causes a rejuvenation of the blood profile (Figures 2O–2S; Figures S2E–S2R; Table S3) and a reversal of the age-dependent decline in the lymphoid-to-myeloid ratio (L/M) (Figure 2 P), as well as of the age-dependent decline in platelets, and hemoglobin (Figures 2Q–2S). Also, 4 months of FMD cycles resulted in an increase in red blood cell count and hemoglobin levels compared to baseline (Figures 2Q–2S). We also measured a panel of 23 cytokines but did not detect changes except for elevated IL-12 and RANTES, as well as reduced GM-CSF in the FMD group (Figures S2S–S2U). These results indicate that chronic use of the FMD promotes immune system regeneration and rejuvenation, in agreement with our previous results on the effect of fasting on lymphocyte number (Cheng et al., 2014).

Among the bone marrow-derived stem cells, hematopoietic stem cells and mesenchymal stem cells represent a potential source for adult tissue and organ regeneration. To investigate whether the rejuvenating effects of the FMD may involve stem cells, we measured hematopoietic (HSPC, $lin^-Scal\text{-}1^+C\text{-}kit^+CD45^+$) and mesenchymal (MSPC, $lin^-Scal\text{-}1^+CD45^-$) stem and progenitor cells in the bone marrow. The number of HSPCs is known to increase with age, possibly to compensate for a reduction in function (Geiger and Van Zant, 2002; Morrison et al., 1996). This age-dependent increase may mask the effects of fasting or FMD in promoting stem cell self-renewal, which we have recently shown for younger mice (Figure S2V) (Cheng et al., 2014). Unlike that of HSPCs, the number of MSPCs declines

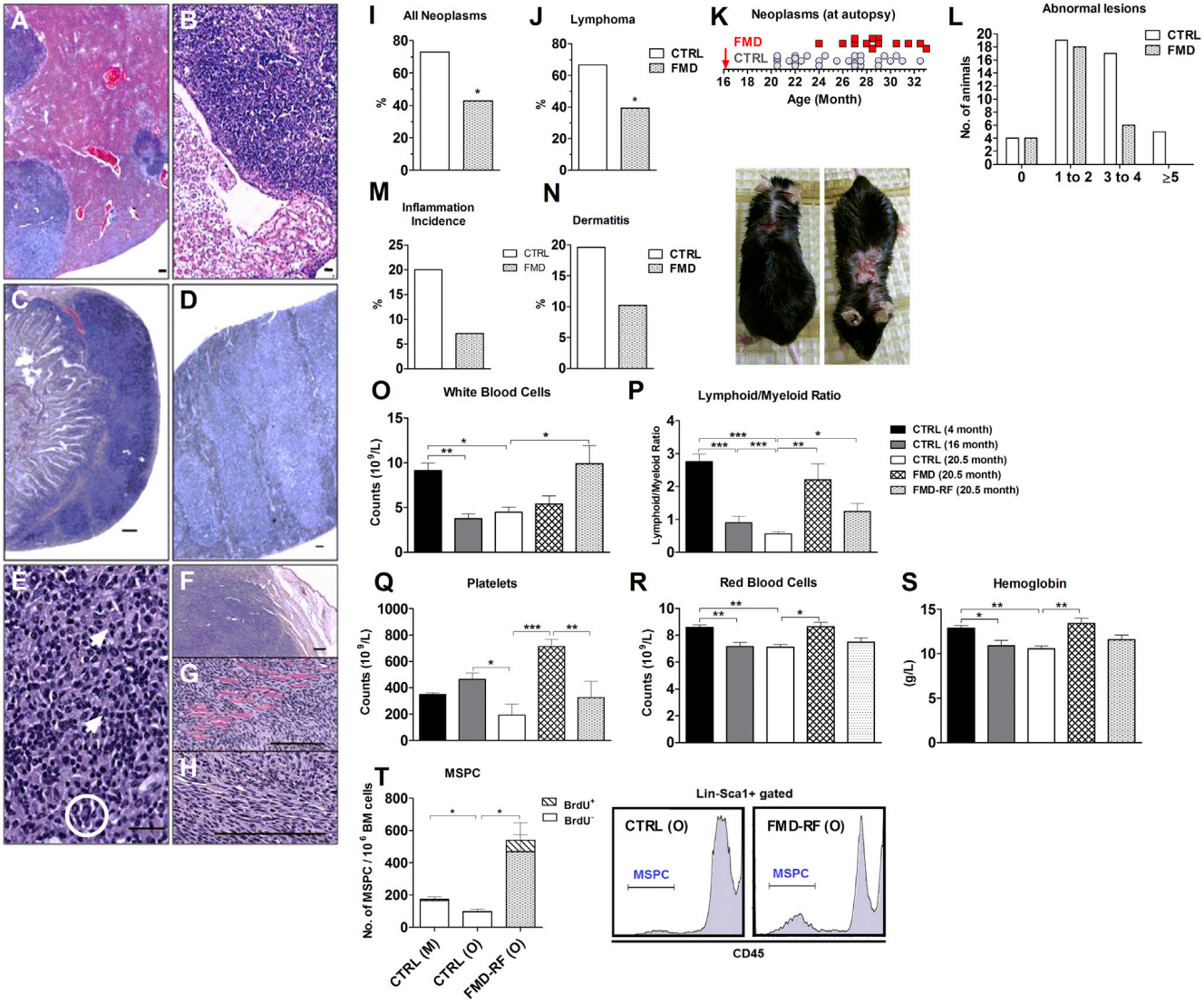

Figure 2. Periodic FMD Cycle Reduces and Delays Cancer, Rejuvenates the Hematopoietic System, and Induces Mesenchymal Stem/Progenitor Cells

(A) Hepatic lymphomatous nodules (bar, 400 microns).

(B–D) Lymphoma in the renal medulla (bar, 100 microns) (B), in a mesenteric lymph node (bar, 100 microns) (C), and in the spleen (bar, 100 microns) (D).

(E) Hepatic lymphoma containing atypical cells with abnormal DNA (circle) and mitosis (arrows, bar, 100 microns).

(F and G) Subcutaneous fibrosarcoma in relationship to the epidermis (F) and with invasion into the skeletal muscle tissue (G).

(H) Cytological details (bar, 100 microns).

(I) Autopsy-confirmed neoplasms.

(J) Lymphoma incidence.

(K) Neoplasms in relationship to the onset (arrow) of the FMD diet.

(L) Number of animals with 0 to greater than 5 abnormal lesions determined at autopsy.

(M) Inflammatory incidence.

(N) Dermatitis incidence in percentage. Images show progression of dermatitis.

(O–S) The number of white blood cells (O), the lymphoid:myeloid ratio (P), as well as the number of platelets (Q), red blood cells (R), and hemoglobin (S) are shown. n = 7–12/group. Other complete blood count parameters are summarized in Figure S2 and Table S3.

(T) lin$^-$Scal-1$^+$CD45$^-$ mesenchymal stem/progenitor cells (MSPC) in bone marrow cells from control mature (M, 8–10 month), old (O, 20.5 month), and FMD mice 7 days after refeeding (FMD-RF; 20.5 month). n = 4–5/group.

All data are expressed as the mean ± SEM.

with age (Bellantuono et al., 2009; Kasper et al., 2009). We confirmed this age-dependent decline comparing MSPC number in mature (8–10 months) and 20.5-month-old mice (Figure 2T), in agreement with previous reports (Kasper et al., 2009; Ratajczak et al., 2008). The number of MSPCs increased 5-fold in the FMD cohort (469.8 ± 179.5 FMD versus 95.5 ± 16.7 CTRL; Figures 2T

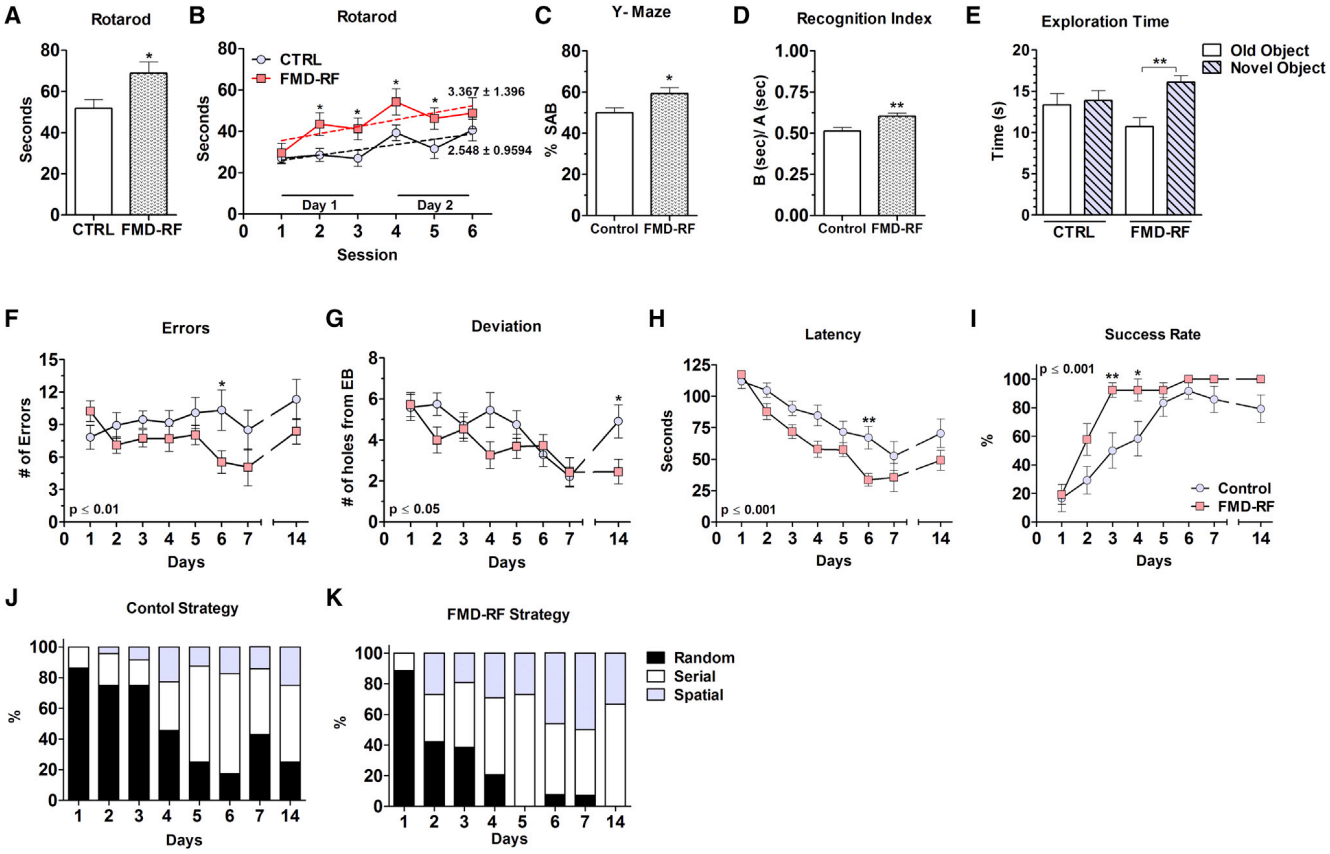

Figure 3. Periodic FMD Cycle Improves Motor Coordination, Hippocampal-Dependent Learning, and Short- and Long-Term Memory

(A) Best rotarod performance score at 23 months. n = 18/group.

(B) Rotarod performance as linear regression for each cohort (dashed lines). n = 18/group.

(C) Spontaneous alternation behavior (SAB) at 23 months. n = 11/group.

(D) Recognition index at 23 months in the novel object recognition task.

(E) Exploration time of the old versus novel object (New, dashed bar). n = 8/group.

(F–I) Error number (F), deviation (G), latency (H), and success rate (I) in the Barnes maze at 23 months. n = 7–12/group.

(J and K) Control (J) and FMD-RF (K) strategies used to locate escape box.

All data are expressed as the mean ± SEM.

and S2W), and that of BrdU$^+$ MSPCs increased by 45-fold in FMD-treated mice (69.8 ± 34.0 FMD versus 1.5 ± 0.6 CTRL) (Figures 2T and S2X). Taken together, these data suggest that cycles of FMD are effective in promoting increases in hematopoietic and mesenchymal stem and progenitor cells, which are likely to contribute to the regeneration of various cell types/systems.

Effects of the FMD on Motor Coordination, Memory, and Neurogenesis

Aging is associated with the decline in locomotor and cognitive function (Lynch, 2004). To evaluate motor coordination and balance, we tested mouse performance on the accelerating rotarod (Shiotsuki et al., 2010). 23-month-old mice fed the FMD every 2 weeks (FMD-RF, tested 1 week after resuming the normal diet) were able to stay longer on the rotarod than mice in the control diet group (Figure 3A). We also assessed motor learning ability by examining performance improvement during subsequent trials. The mice from the FMD-RF group performed consistently better by staying on the accelerating rod longer than mice on the ad libitum diet, although the rate of learning was similar in the two groups (sessions 2–5; Figure 3B). Mouse body weight and best rotarod performance were negatively associated (Pearson correlation coefficient $r = -0.46$; $p = 0.005$). When corrected for weight, rotarod performance improvement was no longer significant ($p = 0.34$; data not shown), indicating that the FMD mice benefit from the fat loss.

To test the effect of the diet on cognitive performance, we carried out working memory tests (Beninger et al., 1986) at 23 months of age (Figure 3C). Mice in the FMD cohort displayed enhanced spontaneous alternating behavior compared to control mice, with no difference in the total number of arm entries (a measure of activity) (Figure S3A). Short-term cognitive performance and context-dependent memory were assessed with the novel object recognition test (Figures 3D and 3E) (Bernabeu et al., 1995). FMD mice had a higher recognition index (RI = 0.60) compared to controls (RI = 0.52; $p < 0.01$) (Figure 3D). An increase in exploration time was observed for the FMD mice for the new object, while the total exploration time remained the same (13.6 ± 0.9 CTRL versus 13.4 ± 0.9 FMD-RF), suggesting enhanced short-term cognitive performance, not general activity (Figure 3E; Figure S3B).

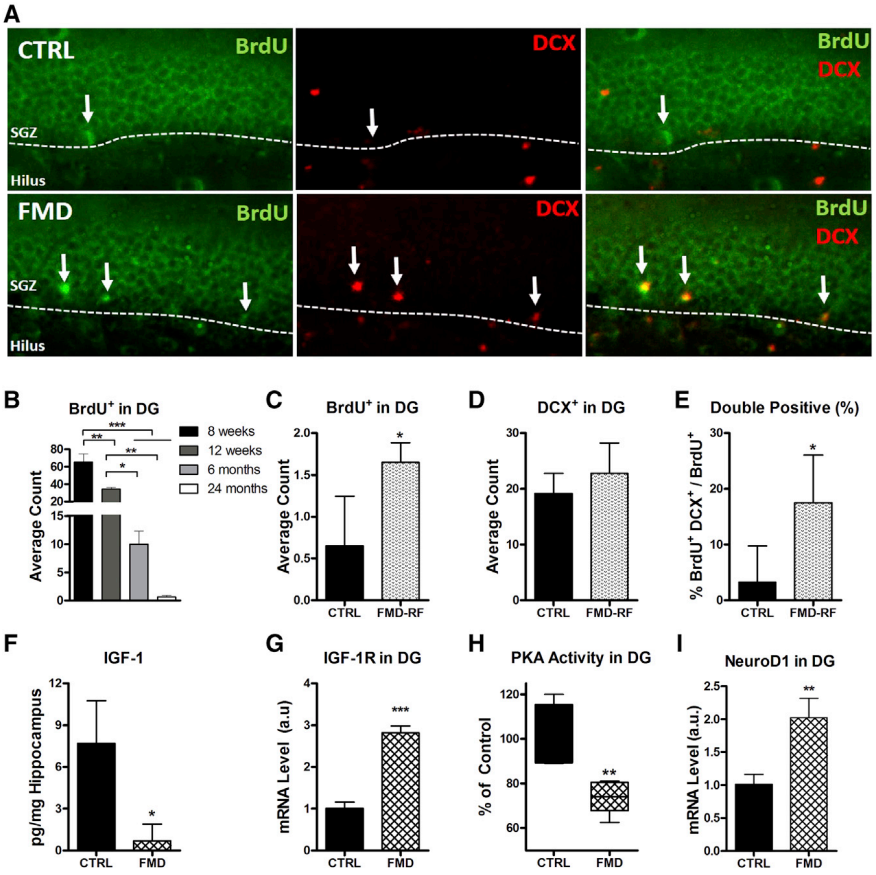

Figure 4. Periodic FMD Cycle Promotes Adult Neurogenesis

(A) Hippocampal immunohistochemistry of control (top row) and FMD (bottom row, see Experimental Procedures for details)-fed 23-month-old animals for BrdU (left, green), DCX (middle, red), and $BrdU^+$ DCX^+ (right).

(B) Age-dependent $BrdU^+$ cell counts in sub-granular zone of the dentate gyrus (DG) (n = 4/group).

(C) $BrdU^+$ cells in the DG at the end of the FMD (n = 4/group).

(D) DCX^+ staining in the DG in 23-month-old animals (n = 4/group).

(E) Percentage of double-positive $BrdU^+$ DCX^+ cells in the DG (n = 4/group).

(F) Hippocampal IGF-1 level after FMD (n = 3/group).

(G) IGF-1R mRNA level in the DG (n = 3/group).

(H) PKA activity level in the DG (n = 5/group).

(I) NeuroD1 mRNA level in the DG (n = 3/group).

All data are expressed as the mean ± SEM.

As a measure of long-term memory, we measured spatial learning and memory using the Barnes maze: a hippocampus-dependent cognitive task requiring spatial reference memory to locate a unique escape box by learning and memorizing visual clues (Figures 3F–3K) (Barnes, 1988). During the 7-day training period, FMD mice performed better with regard to errors, deviation, latency, and success rate compared to controls (Figures 3F–3I). In the retention test, the FMD group displayed better memory indicated by reduced deviation at day 14 (Figure 3G). Deviation of control diet mice at day 14 was similar to that at day 1, indicating that these mice did not remember the box location they had learned by day 7. Improvements in the search strategy, including the shifting from a random and serial search strategy to spatial strategies, were observed for the FMD, but not the control diet group after days 3–4 (Figures 3J and 3K). Together, the behavioral tests suggests that FMD cycles improve motor learning and hippocampus-dependent short- and long-term memory in old animals.

Adult neurogenesis plays an important role in learning and memory (Clelland et al., 2009; Deng et al., 2010; Mattson, 2012). To determine whether the diet affected neurogenesis, we measured BrdU incorporation in the subgranular layer of control mice at the age of 8 weeks, 12 weeks, 6 months, and 24 months (Figure 4B). Similarly to previously reported data, we observed an age-dependent decline in BrdU incorporation in the dentate gyrus (Lee et al., 2012c) (Figure 4B). To assess whether the cognitive improvements in the FMD group are associated with neural regeneration, we measured the proliferative index of DCX^+ immature neurons in the sub-granular cell layer of the dentate gyrus. $BrdU^+$ or $BrdU^+$ DCX^+ double-labeling indicated an increased proliferation of immature neurons in the FMD group compared to that in controls (Figures 4C–4E). To investigate mechanisms of FMD-induced neurogenesis, we fed 6-month-old mice, in which cellular proliferation in the dentate gyrus is reduced by more than 50% compared to that in 8-week-old mice (Figure 4B), with a single cycle of the FMD. After 72 hr on the FMD, we observed a reduction in circulating (Figure S1E) and hippocampal IGF-1 (Figure 4F) but increased IGF-1 receptor mRNA expression in the dentate gyrus region of the hippocampal formation (Figure 4G). Microdissected dentate gyrus-enriched samples from FMD mice displayed a major reduction in PKA activity (Figure 4H) and a 2-fold induction in the expression of NeuroD1 (Figure 4I), a transcription factor important for neuronal protection and differentiation (Gao et al., 2009). Similarly, a single cycle of the FMD increased radial glia-like cells (type I) and non-radial precursor (type II) neural stem cells (Figures S4B, S4C, S4F, and S4G), immature neurons (Figures S4D and S4I–S4Q), and the dendrite-covered area (Figures S4E and S4H) in CD-1 mice.

These results in two genetic backgrounds indicate that the FMD promotes neurogenesis in adult mice. Notably, the brain did not undergo a measurable weight reduction during the FMD, indicating that regeneration can also occur independently of the organ size increase after refeeding. Thus, we hypothesize that alterations in circulating factors, such as the reduction in IGF-1 levels and PKA signaling, can induce pro-regenerative changes that are both dependent and independent of the major cell proliferation that occurs during re-feeding, in agreement with our previous finding in bone marrow and blood cells (Cheng et al., 2014). Most likely, the increase in IGF-1 and PKA after re-feeding also contributes to the proliferative and regenerative process, raising the possibility that both low and high levels of

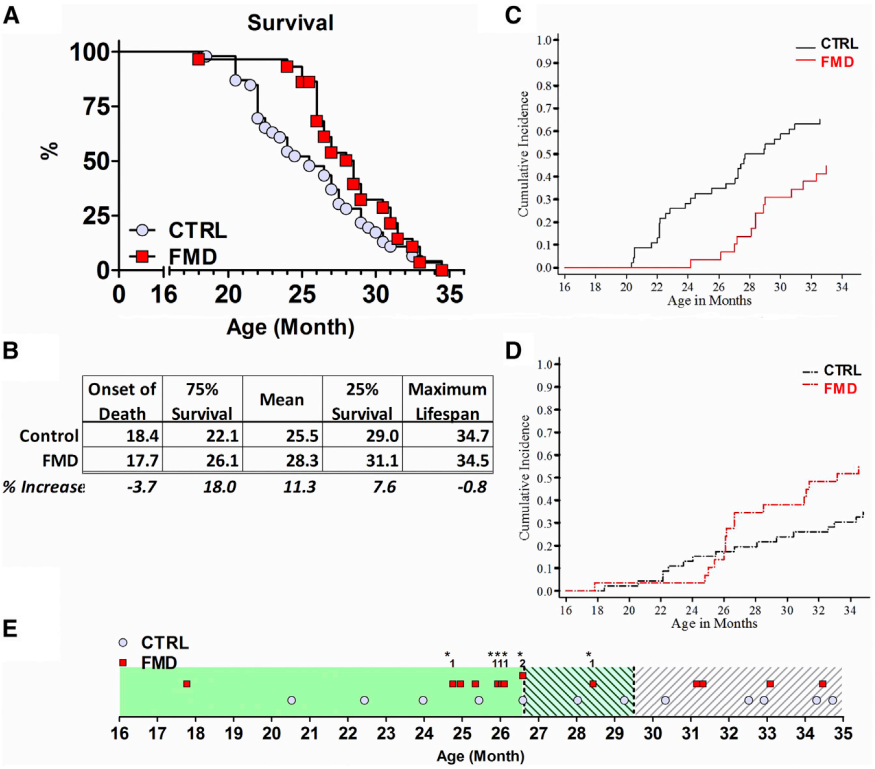

	Onset of Death	75% Survival	Mean	25% Survival	Maximum Lifespan
Control	18.4	22.1	25.5	29.0	34.7
FMD	17.7	26.1	28.3	31.1	34.5
% Increase	*-3.7*	*18.0*	*11.3*	*7.6*	*-0.8*

Figure 5. Periodic FMD Cycle Increases Median Lifespan, but Does Not Affect Maximum Lifespan

(A) Kaplan-Meier survival curve for control and FMD cohort (n = 46 and 29, respectively).

(B) Overview for onset of death, 75%, median, 25%, and maximum lifespan in months with percent change.

(C) Cumulative incidence rates of deaths associated with neoplasia.

(D) Cumulative incidence rates of deaths not associated with neoplasia.

(E) Overview over the date of death not associated with neoplasms. The change from the 4-day FMD to 3-day FMD is indicated by the green shaded area at 26.6 months. The stop of the 3 day FMD and switch to the ad libitum control diet after 6 FMD cycles is indicated by the white shaded area. Numbers over the red squares indicate the number of animals deceased on the particular date; asterisk indicates that death during the FMD regime or within 3 days of refeeding.

All data are expressed as the mean ± SEM.

these proteins can promote regeneration depending on the timing of their expression. Alternatively, the FMD may increase survival of newly differentiated neurons, as observed in the dentate gyrus of alternate day-fed rodents (Lee et al., 2002; Mattson et al., 2001). The observed improvements in cognitive performance in the FMD cohort might be affected by a PKA/CREB-dependent regulation of NeuroD1 (Cho et al., 2012; Sharma et al., 1999), which is known to increase neuronal survival and differentiation of hippocampal progenitors (Roybon et al., 2009), enhance functional integration of new neurons, and alleviate memory deficits in a mouse model of Alzheimer's disease (Richetin et al., 2015).

FMD and Lifespan

Control mice had a median lifespan of 25.5 months (Figure 5A), which was extended to 28.3 months (11% extension) in the FMD group ($p < 0.01$). The FMD showed an 18% extension effect at the 75% survival point, but only a 7.6% extension effect on the 25% survival point and no effect on maximum lifespan (Figures 5A and 5B), indicating that at very advanced ages the 4-day FMD may be beneficial for certain aspects and detrimental for others. Further analysis indicated that many deaths at very old ages occurred during or shortly (within 3 days) after completion of the FMD cycle (Figure 5E, asterisk). Based on this observation, at 26.5 months we shortened the FMD diet from 4 to 3 days and halted the FMD diet completely at 29.5 months. Analyses of the data indicate that whereas the shortening of the FMD from 4 to 3 days was associated with reduced mortality rates between 26.5 and 29.5 months, the halting of the FMD diet at 29.5 months did not reduce mortality further (Figure 5D). These results suggest that FMD cycles can have a potent effect on lifespan and healthspan, but, at least for very old mice, a less-severe (3 versus 4 days) low-calorie and low-protein diet may be preferable to continue to provide beneficial effects while minimizing malnourishment, in agreement with our recent work demonstrating opposite roles of high protein intake on health/mortality in mice and humans of middle to old and very old ages (Levine et al., 2014).

Periodic FMD in a Pilot Randomized Clinical Trial

Markers of Aging and Diseases

To evaluate the feasibility and potential impact of a periodic low-protein and low-calorie FMD in humans, we conducted a pilot clinical trial in generally healthy adults. The components and levels of micro- and macro-nutrients in the human FMD were selected based on their ability to reduce IGF-1, increase IGFBP-1, reduce glucose, increase ketone bodies, maximize nourishment, and minimize adverse effects (Figure 6) in agreement with the FMD's effects in mice (Figure S1). The development of the human diet took into account feasibility (e.g., high adherence to the dietary protocol) and therefore was designed to last 5 days every month and to provide between 34% and 54% of the normal caloric intake with a composition of at least 9%–10% proteins, 34%–47% carbohydrates, and 44%–56% fat. Subjects were randomized either to the FMD for 5 days every month for 3 months (3 cycles) or to a control group in which they continued to consume their normal diet (Figure 6A). Subjects were asked to resume their normal diet after the FMD period and were asked to not implement any changes in their dietary or exercise habits. 5% of the subjects were disqualified due to non-compliance to the dietary protocol. 14% of the enrolled subjects withdrew from the study due to non-diet-related reasons (e.g., work- and travel-related scheduling issues). We present results of the pilot randomized clinical trial that includes a set of 19 participants who successfully completed 3 FMD cycles, as well as data for 19 participants who were randomized to continue on their normal diet and serve as controls. The control

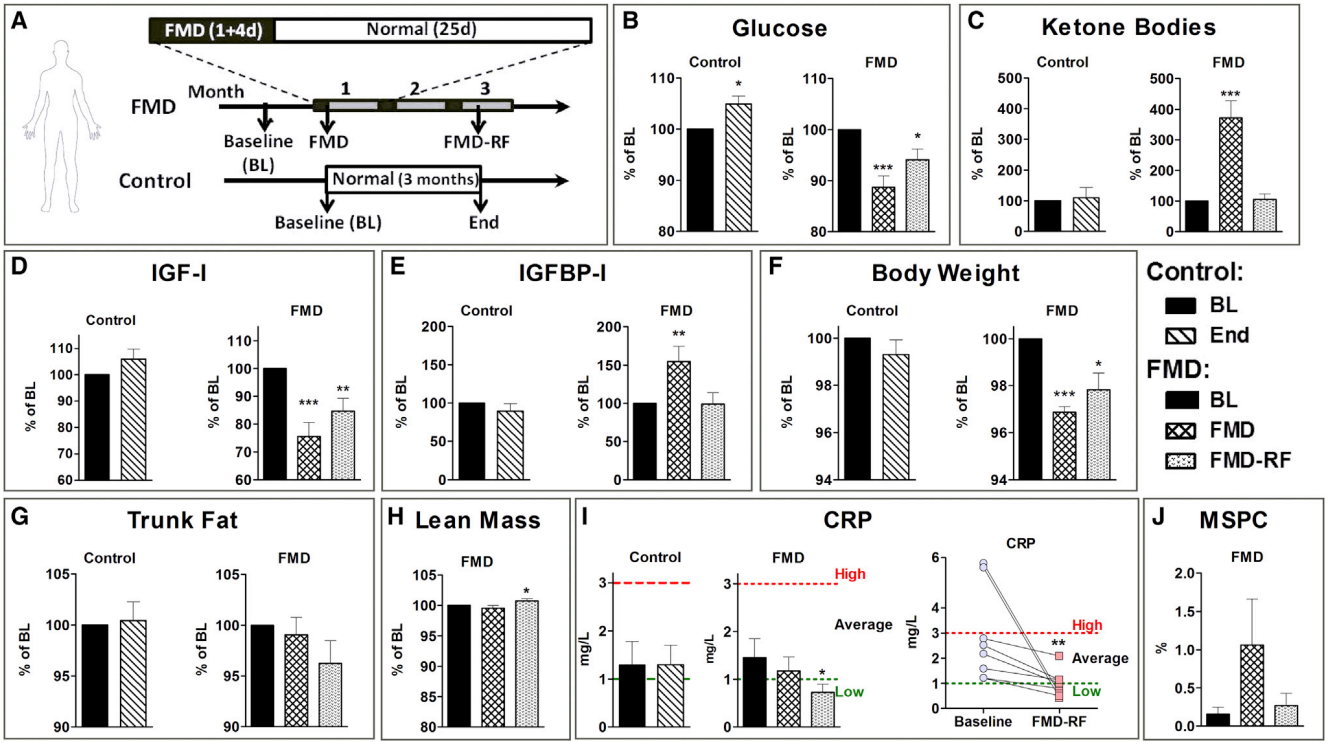

Figure 6. Effects of a Human-Adapted FMD Regimen in a Pilot Clinical Trial

(A) Subjects were randomized to either the fasting mimicking diet (FMD) or a control group. Subjects in the FMD cohort consumed the FMD for 5 consecutive days every month for 3 months and returned to normal diet in between FMDs. Control subjects continued their normal diet. Measurements were performed prior to the diet (Baseline), immediately after the first FMD cycle (FMD), and during the recovery period after the third cycle (FMD-RF). Subjects in the control group were evaluated within the same time frame as the FMD-RF subjects (End).

(B) Glucose (n = 19).

(C) β-hydroxybutyrate (FMD n = 19, Control n = 18).

(D) IGF-1 (FMD n = 19, Control n = 18).

(E) IGFBP-I (FMD n = 19, Control n = 17).

(F) Body weight (n = 19).

(G and H) Trunk fat (FMD n = 18, Control n = 19) (G) and lean body mass (H) evaluated by dual energy X-ray absorptiometry.

(I) C-reactive protein (CRP; FMD n = 19, Control n = 18) levels of all subjects (left) and subjects in the average or high-risk group for heart disease (n = 8; right).

(J) Percentage of $lin^{-}CD184^{+}CD45^{-}$ mesenchymal stem/progenitor cells (MSPC) in the peripheral blood mono-nucleated cell population (FMD n = 16, Control n = 14).

All data are expressed as the mean ± SEM.

group included 9 females (47.4%) and 10 males (52.6%) with an average age of 35.4 ± 5.5 years and 38.0 ± 1.7 years, respectively. The FMD cohort included 7 females (36.8%) and 12 males (63.2%) with an average age of 41.8 ± 4.9 years and 42.5 ± 3.5 years, respectively (Figures S5A and S5B). The age range was 19.8–67.6 years for the control cohort and 27.6–70 years for the FMD cohort. The ethnicity was 58% White, 18.5% Hispanic, 18.5% Asian, and 5% Black (Figure S5C). Subjects were evaluated by a baseline examination (Figure 6A). For the FMD group, the follow-up examinations occurred before resuming normal food intake at the end of the first FMD cycle (FMD) and after 5–8 days of normal dieting following the third FMD cycle (FMD-RF, Figure 6A). The average time between the baseline and the FMD-RF assay/measurement points was 75.2 ± 2.7 days, whereas the time between baseline and the final examination was 74.5 ± 6.0 days in the control group. For all three FMD cycles, study participants self-reported adverse effects following Common Terminology Criteria for Adverse Events (Figure S5D). Adverse effects were higher after completion of the first FMD cycle compared to those during the second and third FMD cycles. However, the average reported severity of the side effects was very low and below "mild" (<1 on a scale of 1–5).

In the FMD subjects, fasting blood glucose levels were reduced by 11.3% ± 2.3% ($p < 0.001$; FMD) and remained 5.9% ± 2.1% lower than baseline levels after resuming the normal diet following the third FMD cycle ($p < 0.05$; Figure 6B). Serum ketone bodies increased 3.7-fold at the end of the FMD regimen ($p < 0.001$) and returned to baseline levels following normal food intake (Figure 6C). Circulating IGF-1 was reduced by ~24% by the end of the FMD period ($p < 0.001$) and remained ~15% lower after resuming the normal diet ($p < 0.01$; Figure 6D). IGFBP-1 was increased 1.5-fold at the end of the FMD regimen ($p < 0.01$) and returned to baseline levels following normal food intake (Figure 6E). These results indicate that the FMD group was highly compliant and generally did not consume foods not included in the FMD box provided to them.

Weight, Abdominal Fat, Lean Body Mass, and Metabolic Markers

In mice, the FMD caused weight loss and reduced visceral fat. We studied whether the FMD could have similar effects in humans by measuring body weight, abdominal fat, and lean body mass. The FMD resulted in a 3% reduction in body weight (3.1% ± 0.3%; $p < 0.001$; Figure 6F) that remained lower at the completion of the study ($p < 0.01$; Figure 6F). Trunk fat percentage, measured by dual-energy X-ray absorptiometry, showed a trend ($p = 0.1$) for reduction after 3 FMD cycles and 1 week of normal dieting (Figure 6G), while the relative lean body mass adjusted for body weight was increased after completion of 3 cycles (Figure 6H), indicating that fat loss accounts for most of the weight loss. Pelvis bone mineral density was not affected by the FMD (Figure S5D).

A complete metabolic panel (Figures S5E–S5L) indicated no persistent metabolic changes due to the FMD except for lowered bilirubin and alkaline phosphatase following the return to the normal diet. Blood urea nitrogen, bilirubin, creatinine, alanine transaminase, and aspartate transaminase showed changes immediately following the FMD, which remained within a safe physiological range. Together with the self-reported Common Terminology Criteria for Adverse Events, these results provide initial evidence that the periodic FMD is generally safe and causes fat loss without reducing lean body mass.

Cardiovascular Disease Risk Factors

In mice, the FMD caused a reduction in inflammation-associated diseases (Figure 2). In humans, the serum level of C-reactive protein (CRP) is a marker of inflammation and risk factor for cardiovascular disease. At baseline, the average CRP level for the FMD subjects was 1.45 ± 0.4 mg/l (Figure 6I) and similar to the control group (1.29 ± 0.5 mg/l), indicating an average moderate risk for cardiovascular disease. CRP levels were reduced by the FMD cycles. 8 of the 19 FMD subjects had CRP levels in the moderate or high cardiovascular disease risk range (levels above 1.0 and 3 mg/l, respectively) at baseline. For 7 of them, the levels returned to the normal range (levels below 1.0 mg/l) after 3 FMD cycles (Figure 6I). For the 11 participants with CRP levels below 1.0 mg/l at baseline, no changes were observed at the completion of the trial. These results indicate that periodic FMD cycles promote anti-inflammatory effects and reduce at least one risk factor for CVD.

Regenerative Markers

In mice, cycles of the FMD promoted an increase of mesenchymal stem and progenitor cells (MSPC; Figure 2). We therefore analyzed $lin^{-}CD184^{+}CD45^{-}$ MSPCs in the peripheral blood of human FMD subjects (Figure 6J). Although not significant, the percentage of MSPC in the peripheral blood mono-nucleated cell population showed a trend ($p = 0.1$) to increase from 0.15 ± 0.1 at baseline to 1.06 ± 0.6 at the end of FMD, with a subsequent return to baseline levels after re-feeding (0.27 ± 0.2). A larger randomized trial will be required to determine whether the number of specific populations of stem cells is in fact elevated by the FMD in humans.

In summary, this study indicates that FMD cycles induce long-lasting beneficial and/or rejuvenating effects on many tissues, including those of the endocrine, immune, and nervous systems in mice and in markers for diseases and regeneration in humans. Although the clinical results will require confirmation by a larger randomized trial, the effects of FMD cycles on biomarkers/risk factors for aging, cancer, diabetes, and CVD, coupled with the very high compliance to the diet and its safety, indicate that this periodic dietary strategy has high potential to be effective in promoting human healthspan. Because prolonged FMDs such as the one tested here are potent and broad-spectrum, they should only be considered for use under medical supervision.

EXPERIMENTAL PROCEDURES

Subjects

Experimental design and report were prepared following the CONSORT standards for randomized clinical trials where applicable. Available data from an ongoing pilot trial are presented. Subjects were recruited under protocols approved by the IRB (HS-12-00391) of the University of Southern California based on established inclusion (generally healthy adult volunteers, 18–70 years of age, BMI: 18.5 and up) and exclusion (any major medical condition and chronic diseases, mental illness, drug dependency, hormone replacement therapy [DHEA, estrogen, thyroid, testosterone], females who are pregnant or nursing, special dietary requirements or food allergies, alcohol dependency) criteria. All participants signed informed consent forms and were not offered financial compensation for participation. Subjects were allocated (based on stratified sampling for age and gender) into a control (n = 19) or experimental diet group (FMD, n = 19), followed by baseline examination. The control group continued normal food consumption and returned for a follow-up examination 3 months after enrollment. Subjects in the FMD cohort consumed the provided experimental diet consisting of 3 cycles of 5 continuous days of FMD followed by 25 days of normal food intake. During all three FMD cycles, study participants self-reported adverse effects following Common Terminology Criteria for Adverse Events. For the FMD group, follow-up examinations occurred before resuming normal food intake at the end of the first cycle (FMD) and also after 5–8 days of normal feeding following the end of the third diet cycle (FMD-RF). Pre-specified outcome measures include adherence to the dietary protocol and evaluation of physiological markers during and after completion of the study. Examinations included height, dressed weight, body composition (including whole-body fat, soft lean tissue, and bone mineral content) measured by dual-energy X-ray absorptiometry (DEXA), and blood draw through venipuncture. All data were collected at the USC Diabetes & Obesity Research Institute. Complete metabolic panels were assayed by the Clinical Laboratories at the Keck Medical Center of USC immediately following blood draw. Data analysis was performed independent of study design. Complete data will be made available elsewhere upon completion of the study.

Human Diet

The human fasting mimicking diet (FMD) program is a plant-based diet program designed to attain fasting-like effects while providing micronutrient nourishment (vitamins, minerals, etc.) and minimize the burden of fasting. It comprises proprietary vegetable-based soups, energy bars, energy drinks, chip snacks, chamomile flower tea, and a vegetable supplement formula tablet (Table S4). The human FMD diet consists of a 5 day regimen: day 1 of the diet supplies ~1,090 kcal (10% protein, 56% fat, 34% carbohydrate), days 2–5 are identical in formulation and provide 725 kcal (9% protein, 44% fat, 47% carbohydrate).

Animals

All animal protocols were approved by the Institutional Animal Care and Use Committee (IACUC) of the University of Southern California. Experimental design and report were prepared following the ARRIVE standards for mouse work. 110 9-month-old female C57Bl/6 (Charles River) retired breeders were maintained in a pathogen-free environment and housed in clear shoebox cages in groups of three animals per cage with constant temperature and humidity and 12 hr/12 hr light/dark cycle and unlimited access to water. At 16 months of age, animals were randomly divided (by cage to avoid fighting) into the ad libitum-fed control (CTRL) group and the fasting mimicking diet (FMD) group. Bodyweight of individual animals was measured routinely every 2 weeks, prior

to starting a new FMD cycle. n = 9 mice were measured daily in the FMD and control cohort for safety evaluation and to establish a weight profile during the FMD cycle. Food intake was measured daily. Upon indication of progressing dermatitis, animals were treated with a triple antibiotic ointment (Fougera Pharmaceuticals) and were euthanized if the condition progressed. To reduce subjective bias, mice were randomly assigned (using the online Random Number Calculator from GraphPad) to any behavioral and physiological assessments shortly before any experiment. Mice that appeared weak and/or showed signs of illness were not included in any experiment. Upon death/sacrifice, autopsies were performed and all abnormal classified lesions submitted for evaluation by a pathologist. Autopsies were performed on 73 mice; 2 mice (one from each cohort, respectively) were cannibalized and not available for autopsy. We also utilized strain-matched younger animals to establish age-dependent changes in risk factors using identical methods. In addition, 6-month-old female CD-1 mice (Charles River) were used in supplemental experiments to measure adult neurogenesis.

Rodent Diets

Mice were fed ad libitum with irradiated TD.7912 rodent chow (Harlan Teklad) containing 15.69 kJ/g of digestible energy (3.92 kJ/g animal-based protein, 9.1 kJ/g carbohydrate, 2.67 kJ/g fat).

The FMD is based on a nutritional screen that identified ingredients that allow nourishment during periods of low calorie consumption (Brandhorst et al., 2013). The FMD consists of two different components designated as day 1 diet and day 2–4 diet that were fed in this respective order. The day 1 diet consists of a mix of various low-calorie broth powders, a vegetable medley powder, extra virgin olive oil, and essential fatty acids; day 2–4 diet consist of low-calorie broth powders and glycerol. Both formulations were then substituted with hydrogel (Clear H2O) to achieve binding and to allow the supply of the food in the cage feeders. Day 1 diet contains 7.67 kJ/g (provided at ~50% of normal daily intake; 0.46 kJ/g protein, 2.2 kJ/g carbohydrate, 5.00 kJ/g fat); the day 2–4 diet is identical on all feeding days and contains 1.48 kJ/g (provided at ~10% of normal daily intake; 0.01 kJ/g protein/fat, 1.47 kJ/g carbohydrates). An alternative FMD containing 0.26 kJ/g (0.01 kJ/g protein/fat, 0.25 kJ/g carbohydrates) was supplied for 3 days for the evaluation of adult neurogenesis. Mice consumed all the supplied food on each day of the FMD regimen and showed no signs of food aversion. At the end of either diet, we supplied TD.7912 chow ad libitum for 10 days before starting another FMD cycle. Prior to the FMD, animals were transferred into fresh cages to avoid feeding on residual chow and coprophagy.

Survival Analysis

The endpoint considered was survival defined as the duration in time between treatment starting date and date of death. Mice showing signs of severe stress, deteriorating health status, or excess tumor load were designated as moribund and euthanized. Two mice in the FMD group were sacrificed due to seizure and head/neck injury, and one mouse died during anesthesia. A total of 75 mice were included in the survival analysis, 46 in the control group, and 29 in the FMD group. 12 were sacrificed due to progressing dermatitis (CTRL n = 9, FMD n = 3) and considered as deaths for the assessment of healthspan. Two cannibalized mice were considered as dead due to reasons other than neoplasia in the analysis. A secondary analysis that considered the 2 mice as dead because of neoplasia rendered similar results (data not shown).

Physiological Biomarkers

Prior to blood collection and glucose measurements, mice were withheld from food for up to 4 hr to avoid interferences caused by food consumption. For mice, blood glucose was measured with the Precision Xtra blood glucose monitoring system (Abbott Laboratories). An overview of all utilized commercial kits is given in the Supplemental Experimental Procedures.

Complete Blood Counts and Cytokines

Complete blood counts were performed using the Mindray BC-2800 VET auto hematology analyzer following the manufacturer's protocol. In brief, blood was collected from the tail vein in heparin-coated micro-hematocrit tubes. 20 μl of the heparinized blood was added to CDS diluent (Clinical Diagnostics Solution), and whole-blood parameters were evaluated. Cytokines were measured using the Bio-Plex Cytokine Assay (Bio-Rad), following the manufacturers recommendation for serum analysis.

Echocardiography

Animals were anesthetized with 2% isoflurane, and the left hemithorax was shaved. The mice were placed on a temperature-controlled heating pad, and heart rate was continuously monitored (400–550 bpm). Ultrasound trans-mission gel (Parker Laboratories) was used, and the heart was imaged in the parasternal short-axis view. 2D B-mode images were obtained at the papillary muscle level using the high-resolution Vevo 770 Ultrasound system (VisualSonics) and analyzed using Vevo 770 V2.2.3 software (VisualSonics).

X-Ray Computed Tomography Scans

Mice (representing average body weight) were anesthetized using 2% inhalant isoflurane and placed in a fixed position on their back. Due to prolonged anesthesia times, animal number was kept at n = 3 to minimize the risk of accidental death of old mice. Tissue bone mineral density (mg Hydroxyapatite/cm^3) of both femora was measured in vivo for n = 5/group using the Siemens InveonCT scanner. A detailed description is given in the Supplemental Experimental Procedures.

Bone Marrow Collection and FACS Analysis

Bone marrow cells were harvested from femurs and tibia of mice in alpha-MEM media (Corning Cellgro). For mice, freshly collected bone marrow cells were washed with PBS and stained with lineage-specific, Scal-1, c-Kit, and BrdU antibodies (BD Biosciences) according to manufacturer's instructions. Analysis was performed using BD FACS diva on LSR II. Human $Lin^-CD184^+CD45^-$ mesenchymal stem/progenitor cells in the peripheral blood mono-nucleated cell population were identified using human hematopoietic lineage FITC cocktail, anti-human CD45 APC, and anti-human CD184-PE (eBioscience, #22-7778-72, #17-9459-42, #12-9999-42).

Immunohistochemistry

For the detection of hematopoietic cell genesis, mice were injected intraperitoneal with 2% filter-sterilized BrdU (10 mg/ml stock solution, Sigma) at a single dose of 200 mg/kg bodyweight in PBS 24 hr prior to the bone marrow collection. To analyze adult neurogenesis, BrdU was injected at 50 mg/kg for 3 or 4 consecutive days (Figure S4) prior to FMD feeding. Staining for BrdU, Ki67, Sox2, GFAP, and doublecortin was performed as described in the Supplemental Experimental Procedures.

Western Blotting

A detailed description is given in the Supplemental Experimental Procedures.

qPCR

Relative transcript expression levels were measured by quantitative real-time PCR as described in the Supplemental Experimental Procedures.

Behavior Studies

A detailed description is given in the Supplemental Experimental Procedures.

Y Maze

11 mice per treatment group were tested at 23 months of age. Spontaneous alternation behavior (SAB) score was calculated as the proportion of alternations (an arm choice differing from the previous two choices) to the total number of alternation opportunities.

Accelerating Rotarod

At 23 months of age, 18 mice/group were evaluated using an accelerating rotarod. The speed and time after which the mice fell off were recorded. On two consecutive days, the mice were given three successive trials, for a total of six trials. Performance was measured with two variables: the mean of the individual best performance over the two consecutive trial days and the mean time the mice of each treatment group remained in balance over the six trial session as an index of training.

Novel Object Recognition

The testing session comprised two trials of 5 min of each. During the first trial (T1), the apparatus contained two identical objects. After a 1 hr delay interval, mice were placed back in the apparatus for the second trial (T2), now with one familiar and one new object. The time spent exploring each object during T1

and T2 was recorded manually. Recognition index was calculated as the time (in seconds) spent between familiar and new object.

Barnes Maze

12 mice/group were tested twice daily for 7 days at 23 months of age. Success rate (100%, finding the escape box [EB] within 2 min; 0%, not finding the EB within 2 min), latency (time to enter the EB), number of errors (nose pokes and head deflections over false holes), deviation (how many holes away from the EB was the first error), and strategies used to locate the EB were recorded and averaged from two tests to obtain daily values. Search strategies were classified as random (crossings through the maze center), serial (searches in clockwise or counter-clockwise direction), or spatial (navigating directly to the EB with both error and deviation scores of no more than 3). Retention was assessed by testing once on day 14.

Yeast Intermittent Fasting

Yeast cells were streaked out from frozen stock onto YPD plates and incubated at 30°C for 2 days. Next, 3–5 colonies were inoculated in 2 ml of liquid SDC and incubated overnight. 100 μl of the overnight culture was added to 10 ml of fresh SDC in a 50 ml flask and incubated at 30°C for 3 days. On day 3, a dilution of the culture was plated on YPD plates to evaluate the number of viable cells. The remaining culture was spun down, media was removed, and the pellet was washed with sterile dH_2O twice before re-suspending in 10 ml of sterile dH_2O in a 50 ml flask followed by incubation for 2 days. On day 5, once again a dilution of the culture was plated on YPD, and the remainder was pelleted and re-suspended in 10 ml of expired media followed by 48 hr incubation. This process was repeated by alternating dH_2O and expired media treatment every 2 days until the number of viable cells reached below 10% of the original culture.

To prepare expired media, 3–5 colonies were inoculated in 5 ml of SDC overnight. 500 μl of the overnight culture was added to 200 ml SDC in a 500 ml flask and incubated in an orbital shaker for 4 days. After the incubation period, the cultures were filtered using a 0.22 micron filter and used for the duration of the experiment.

Statistical Analysis

All data are expressed as the mean ± SEM. For mice, all statistical analyses were two sided, and p values < 0.05 were considered significant (*$p < 0.05$, **$p < 0.01$, ***$p < 0.001$). Differences among groups were tested by either Student's t test comparison, one-way ANOVA followed by Tukey's multiple comparison, or two-way ANOVA (for Barnes maze) using GraphPad Prism v.5. Kaplan-Meier survival curves were compared using the Gehan-Breslow-Wilcoxon test. Competing risk analysis was performed to assess statistical differences in the rate of deaths. For human subjects, statistical analysis was performed using the Wilcoxon signed-rank test, and p values < 0.05 were considered significant (*$p < 0.05$, **$p < 0.01$, ***$p < 0.001$).

SUPPLEMENTAL INFORMATION

Supplemental Information includes Supplemental Experimental Procedures, five figures, and four tables and can be found with this article online at http://dx.doi.org/10.1016/j.cmet.2015.05.012.

AUTHOR CONTRIBUTIONS

Preclinical studies: S.B. and I.Y.C., collected and analyzed the data. H.M. and M.G.M. performed the yeast experiments. G.N. and C.W.C. collected and processed the CBC data. C.W.C. performed FACS analysis. S.S. performed creatinine, BUN, ALT, and renal histology. L.D. performed autopsies and histology. L.P.Y. and R.P. performed X-ray computed tomography. L.P.Y., R.P., and M.V. performed echocardiography. S.D.B. performed cytokine assay. F.P. performed protein expression for autophagy and myogenesis. L.J. and S.G. performed bioinformatics analyses. P.O., L.P., P.S.C., Y.I., B.K.K., and P.C. were involved in study design. S.B., T.E.M., and V.D.L. designed the mouse study. V.D.L. supervised all yeast and mouse studies. Clinical trial: V.D.L and M.W. designed the clinical trial. V.D.L., M.W., and T.B.D. supervised the clinical trial. M.W. and T.B.D. performed data collection and analysis together with S.B., S.G., and H.M. S.B., I.Y.C., and V.D.L. wrote the paper. S.B. and I.Y.C. contributed equally to this work. All authors discussed the results and commented on the manuscript.

CONFLICT OF INTEREST

V.D.L. and T.E.M. have equity interest in L-Nutra, a company that develops medical food. 100% of the L-Nutra equity belonging to V.D.L. will be donated to non-profit organizations. Neither author had any role in data analysis.

ACKNOWLEDGMENTS

We would like to thank Giusi Taormina, Shawna Chagoury, and Lynn Baufeld for their assistance in the yeast chronological lifespan experiments. Funding was provided by the NIH and NIA grants (AG20642, AG025135, AG034906), The Bakewell Foundation, The V Foundation for Cancer Research, and a USC Norris Cancer Center pilot grant to V.D.L. The human study was funded by the USC Edna Jones chair fund. The Molecular Imaging Center at USC is supported in part by the National Center for Research Resources (NCRR, S10RR017964-01). The funding sources had no involvement in study design; in the collection, analysis, and interpretation of data; in the writing of the report; or in the decision to submit the article for publication. The content is solely the responsibility of the authors and does not necessarily represent the official views of the National Institute on Aging or the NIH. The University of Southern California has licensed intellectual property to L-Nutra that is under study in this research. As part of this license agreement, the University has the potential to receive royalty payments from L-Nutra.

Received: February 2, 2015
Revised: April 2, 2015
Accepted: May 8, 2015
Published: June 18, 2015

REFERENCES

Antosh, M., Whitaker, R., Kroll, A., Hosier, S., Chang, C., Bauer, J., Cooper, L., Neretti, N., and Helfand, S.L. (2011). Comparative transcriptional pathway bioinformatic analysis of dietary restriction, Sir2, p53 and resveratrol life span extension in Drosophila. Cell Cycle *10*, 904–911.

Barnes, C.A. (1988). Spatial learning and memory processes: the search for their neurobiological mechanisms in the rat. Trends Neurosci. *11*, 163–169.

Bartke, A., Sun, L.Y., and Longo, V. (2013). Somatotropic signaling: trade-offs between growth, reproductive development, and longevity. Physiol. Rev. *93*, 571–598.

Bellantuono, I., Aldahmash, A., and Kassem, M. (2009). Aging of marrow stromal (skeletal) stem cells and their contribution to age-related bone loss. Biochim. Biophys. Acta *1792*, 364–370.

Beninger, R.J., Jhamandas, K., Boegman, R.J., and el-Defrawy, S.R. (1986). Effects of scopolamine and unilateral lesions of the basal forebrain on T-maze spatial discrimination and alternation in rats. Pharmacol. Biochem. Behav. *24*, 1353–1360.

Bernabeu, R., de Stein, M.L., Fin, C., Izquierdo, I., and Medina, J.H. (1995). Role of hippocampal NO in the acquisition and consolidation of inhibitory avoidance learning. Neuroreport *6*, 1498–1500.

Blackwell, B.N., Bucci, T.J., Hart, R.W., and Turturro, A. (1995). Longevity, body weight, and neoplasia in ad libitum-fed and diet-restricted C57BL6 mice fed NIH-31 open formula diet. Toxicol. Pathol. *23*, 570–582.

Blagosklonny, M.V., Campisi, J., and Sinclair, D.A. (2009). Aging: past, present and future. Aging (Albany, N.Y. Online) *1*, 1–5.

Brandhorst, S., Wei, M., Hwang, S., Morgan, T.E., and Longo, V.D. (2013). Short-term calorie and protein restriction provide partial protection from chemotoxicity but do not delay glioma progression. Exp. Gerontol. *48*, 1120–1128.

Brown-Borg, H.M. (2009). Hormonal control of aging in rodents: the somatotropic axis. Mol. Cell. Endocrinol. *299*, 64–71.

Cheng, C.-W., Adams, G.B., Perin, L., Wei, M., Zhou, X., Lam, B.S., Da Sacco, S., Mirisola, M., Quinn, D.I., Dorff, T.B., et al. (2014). Prolonged fasting reduces IGF-1/PKA to promote hematopoietic-stem-cell-based regeneration and reverse immunosuppression. Cell Stem Cell *14*, 810–823.

Cho, I.S., Jung, M., Kwon, K.S., Moon, E., Cho, J.H., Yoon, K.H., Kim, J.W., Lee, Y.D., Kim, S.S., and Suh-Kim, H. (2012). Deregulation of CREB signaling

pathway induced by chronic hyperglycemia downregulates NeuroD transcription. PLoS ONE *7*, e34860.

Clelland, C.D., Choi, M., Romberg, C., Clemenson, G.D., Jr., Fragniere, A., Tyers, P., Jessberger, S., Saksida, L.M., Barker, R.A., Gage, F.H., and Bussey, T.J. (2009). A functional role for adult hippocampal neurogenesis in spatial pattern separation. Science *325*, 210–213.

Conboy, I.M., and Rando, T.A. (2012). Heterochronic parabiosis for the study of the effects of aging on stem cells and their niches. Cell Cycle *11*, 2260–2267.

Coppé, J.P., Desprez, P.Y., Krtolica, A., and Campisi, J. (2010). The senescence-associated secretory phenotype: the dark side of tumor suppression. Annu. Rev. Pathol. *5*, 99–118.

Cuervo, A.M., Bergamini, E., Brunk, U.T., Dröge, W., Ffrench, M., and Terman, A. (2005). Autophagy and aging: the importance of maintaining "clean" cells. Autophagy *1*, 131–140.

Deng, W., Aimone, J.B., and Gage, F.H. (2010). New neurons and new memories: how does adult hippocampal neurogenesis affect learning and memory? Nat. Rev. Neurosci. *11*, 339–350.

Fabrizio, P., Pozza, F., Pletcher, S.D., Gendron, C.M., and Longo, V.D. (2001). Regulation of longevity and stress resistance by Sch9 in yeast. Science *292*, 288–290.

Fontana, L., Partridge, L., and Longo, V.D. (2010). Extending healthy life span—from yeast to humans. Science *328*, 321–326.

Gao, Z., Ure, K., Ables, J.L., Lagace, D.C., Nave, K.A., Goebbels, S., Eisch, A.J., and Hsieh, J. (2009). Neurod1 is essential for the survival and maturation of adult-born neurons. Nat. Neurosci. *12*, 1090–1092.

Geiger, H., and Van Zant, G. (2002). The aging of lympho-hematopoietic stem cells. Nat. Immunol. *3*, 329–333.

Gems, D., and Partridge, L. (2013). Genetics of longevity in model organisms: debates and paradigm shifts. Annu. Rev. Physiol. *75*, 621–644.

Greer, E.L., and Brunet, A. (2009). Different dietary restriction regimens extend lifespan by both independent and overlapping genetic pathways in C. elegans. Aging Cell *8*, 113–127.

Guarente, L., and Kenyon, C. (2000). Genetic pathways that regulate ageing in model organisms. Nature *408*, 255–262.

Haigis, M.C., and Yankner, B.A. (2010). The aging stress response. Mol. Cell *40*, 333–344.

Harrison, D.E., Strong, R., Sharp, Z.D., Nelson, J.F., Astle, C.M., Flurkey, K., Nadon, N.L., Wilkinson, J.E., Frenkel, K., Carter, C.S., et al. (2009). Rapamycin fed late in life extends lifespan in genetically heterogeneous mice. Nature *460*, 392–395.

Harvie, M.N., Pegington, M., Mattson, M.P., Frystyk, J., Dillon, B., Evans, G., Cuzick, J., Jebb, S.A., Martin, B., Cutler, R.G., et al. (2011). The effects of intermittent or continuous energy restriction on weight loss and metabolic disease risk markers: a randomized trial in young overweight women. Int J Obes (Lond) *35*, 714–727.

Johnson, T.E., Cypser, J., de Castro, E., de Castro, S., Henderson, S., Murakami, S., Rikke, B., Tedesco, P., and Link, C. (2000). Gerontogenes mediate health and longevity in nematodes through increasing resistance to environmental toxins and stressors. Exp. Gerontol. *35*, 687–694.

Junnila, R.K., List, E.O., Berryman, D.E., Murrey, J.W., and Kopchick, J.J. (2013). The GH/IGF-1 axis in ageing and longevity. Nat. Rev. Endocrinol. *9*, 366–376.

Kaeberlein, T.L., Smith, E.D., Tsuchiya, M., Welton, K.L., Thomas, J.H., Fields, S., Kennedy, B.K., and Kaeberlein, M. (2006). Lifespan extension in Caenorhabditis elegans by complete removal of food. Aging Cell *5*, 487–494.

Kasper, G., Mao, L., Geissler, S., Draycheva, A., Trippens, J., Kühnisch, J., Tschirschmann, M., Kaspar, K., Perka, C., Duda, G.N., and Klose, J. (2009). Insights into mesenchymal stem cell aging: involvement of antioxidant defense and actin cytoskeleton. Stem Cells *27*, 1288–1297.

Katsimpardi, L., Litterman, N.K., Schein, P.A., Miller, C.M., Loffredo, F.S., Wojtkiewicz, G.R., Chen, J.W., Lee, R.T., Wagers, A.J., and Rubin, L.L. (2014). Vascular and neurogenic rejuvenation of the aging mouse brain by young systemic factors. Science *344*, 630–634.

Komatsu, M., Waguri, S., Koike, M., Sou, Y.S., Ueno, T., Hara, T., Mizushima, N., Iwata, J., Ezaki, J., Murata, S., et al. (2007). Homeostatic levels of p62 control cytoplasmic inclusion body formation in autophagy-deficient mice. Cell *131*, 1149–1163.

Lee, J., Duan, W., and Mattson, M.P. (2002). Evidence that brain-derived neurotrophic factor is required for basal neurogenesis and mediates, in part, the enhancement of neurogenesis by dietary restriction in the hippocampus of adult mice. J. Neurochem. *82*, 1367–1375.

Lee, C., Safdie, F.M., Raffaghello, L., Wei, M., Madia, F., Parrella, E., Hwang, D., Cohen, P., Bianchi, G., and Longo, V.D. (2010). Reduced levels of IGF-I mediate differential protection of normal and cancer cells in response to fasting and improve chemotherapeutic index. Cancer Res. *70*, 1564–1572.

Lee, C., Raffaghello, L., Brandhorst, S., Safdie, F.M., Bianchi, G., Martin-Montalvo, A., Pistoia, V., Wei, M., Hwang, S., Merlino, A., et al. (2012a). Fasting cycles retard growth of tumors and sensitize a range of cancer cell types to chemotherapy. Sci. Transl. Med. *4*, 24ra27.

Lee, C., Raffaghello, L., and Longo, V.D. (2012b). Starvation, detoxification, and multidrug resistance in cancer therapy. Drug Resist. Updat. *15*, 114–122.

Lee, S.W., Clemenson, G.D., and Gage, F.H. (2012c). New neurons in an aged brain. Behav. Brain Res. *227*, 497–507.

Levine, M.E., Suarez, J.A., Brandhorst, S., Balasubramanian, P., Cheng, C.W., Madia, F., Fontana, L., Mirisola, M.G., Guevara-Aguirre, J., Wan, J., et al. (2014). Low protein intake is associated with a major reduction in IGF-1, cancer, and overall mortality in the 65 and younger but not older population. Cell Metab. *19*, 407–417.

Longo, V.D., and Finch, C.E. (2003). Evolutionary medicine: from dwarf model systems to healthy centenarians? Science *299*, 1342–1346.

Longo, V.D., and Mattson, M.P. (2014). Fasting: molecular mechanisms and clinical applications. Cell Metab. *19*, 181–192.

López-Otín, C., Blasco, M.A., Partridge, L., Serrano, M., and Kroemer, G. (2013). The hallmarks of aging. Cell *153*, 1194–1217.

Lynch, M.A. (2004). Long-term potentiation and memory. Physiol. Rev. *84*, 87–136.

Madeo, F., Tavernarakis, N., and Kroemer, G. (2010). Can autophagy promote longevity? Nat. Cell Biol. *12*, 842–846.

Mair, W., and Dillin, A. (2008). Aging and survival: the genetics of life span extension by dietary restriction. Annu. Rev. Biochem. *77*, 727–754.

Mattson, M.P. (2012). Energy intake and exercise as determinants of brain health and vulnerability to injury and disease. Cell Metab. *16*, 706–722.

Mattson, M.P., Duan, W., Lee, J., and Guo, Z. (2001). Suppression of brain aging and neurodegenerative disorders by dietary restriction and environmental enrichment: molecular mechanisms. Mech. Ageing Dev. *122*, 757–778.

Morgan, T.E., Wong, A.M., and Finch, C.E. (2007). Anti-inflammatory mechanisms of dietary restriction in slowing aging processes. Interdiscip. Top. Gerontol. *35*, 83–97.

Morrison, S.J., Wandycz, A.M., Akashi, K., Globerson, A., and Weissman, I.L. (1996). The aging of hematopoietic stem cells. Nat. Med. *2*, 1011–1016.

Moscat, J., and Diaz-Meco, M.T. (2011). Feedback on fat: p62-mTORC1-autophagy connections. Cell *147*, 724–727.

Muller-Sieburg, C.E., Cho, R.H., Karlsson, L., Huang, J.F., and Sieburg, H.B. (2004). Myeloid-biased hematopoietic stem cells have extensive self-renewal capacity but generate diminished lymphoid progeny with impaired IL-7 responsiveness. Blood *103*, 4111–4118.

Narasimhan, S.D., Yen, K., and Tissenbaum, H.A. (2009). Converging pathways in lifespan regulation. Curr. Biol. *19*, R657–R666.

Olguin, H.C., Yang, Z., Tapscott, S.J., and Olwin, B.B. (2007). Reciprocal inhibition between Pax7 and muscle regulatory factors modulates myogenic cell fate determination. J. Cell Biol. *177*, 769–779.

Perry, R.L., and Rudnick, M.A. (2000). Molecular mechanisms regulating myogenic determination and differentiation. Front. Biosci. *5*, D750–D767.

Raffaghello, L., Lee, C., Safdie, F.M., Wei, M., Madia, F., Bianchi, G., and Longo, V.D. (2008). Starvation-dependent differential stress resistance

protects normal but not cancer cells against high-dose chemotherapy. Proc. Natl. Acad. Sci. USA *105*, 8215–8220.

Ratajczak, M.Z., Zuba-Surma, E.K., Wysoczynski, M., Ratajczak, J., and Kucia, M. (2008). Very small embryonic-like stem cells: characterization, developmental origin, and biological significance. Exp. Hematol. *36*, 742–751.

Richetin, K., Leclerc, C., Toni, N., Gallopin, T., Pech, S., Roybon, L., and Rampon, C. (2015). Genetic manipulation of adult-born hippocampal neurons rescues memory in a mouse model of Alzheimer's disease. Brain *138*, 440–455.

Roybon, L., Hjalt, T., Stott, S., Guillemot, F., Li, J.Y., and Brundin, P. (2009). Neurogenin2 directs granule neuroblast production and amplification while NeuroD1 specifies neuronal fate during hippocampal neurogenesis. PLoS ONE *4*, e4779.

Schnell, M.A., Hardy, C., Hawley, M., Propert, K.J., and Wilson, J.M. (2002). Effect of blood collection technique in mice on clinical pathology parameters. Hum. Gene Ther. *13*, 155–161.

Sharma, A., Moore, M., Marcora, E., Lee, J.E., Qiu, Y., Samaras, S., and Stein, R. (1999). The NeuroD1/BETA2 sequences essential for insulin gene transcription colocalize with those necessary for neurogenesis and p300/CREB binding protein binding. Mol. Cell. Biol. *19*, 704–713.

Shaw, A.C., Joshi, S., Greenwood, H., Panda, A., and Lord, J.M. (2010). Aging of the innate immune system. Curr. Opin. Immunol. *22*, 507–513.

Shen, J., Tsai, Y.T., Dimarco, N.M., Long, M.A., Sun, X., and Tang, L. (2011). Transplantation of mesenchymal stem cells from young donors delays aging in mice. Sci Rep *1*, 67.

Shi, Y., Felley-Bosco, E., Marti, T.M., Orlowski, K., Pruschy, M., and Stahel, R.A. (2012). Starvation-induced activation of ATM/Chk2/p53 signaling sensitizes cancer cells to cisplatin. BMC Cancer *12*, 571.

Shiotsuki, H., Yoshimi, K., Shimo, Y., Funayama, M., Takamatsu, Y., Ikeda, K., Takahashi, R., Kitazawa, S., and Hattori, N. (2010). A rotarod test for evaluation of motor skill learning. J. Neurosci. Methods *189*, 180–185.

Sinha, M., Jang, Y.C., Oh, J., Khong, D., Wu, E.Y., Manohar, R., Miller, C., Regalado, S.G., Loffredo, F.S., Pancoast, J.R., et al. (2014). Restoring systemic GDF11 levels reverses age-related dysfunction in mouse skeletal muscle. Science *344*, 649–652.

Smith, E.D., Kaeberlein, T.L., Lydum, B.T., Sager, J., Welton, K.L., Kennedy, B.K., and Kaeberlein, M. (2008). Age- and calorie-independent life span extension from dietary restriction by bacterial deprivation in Caenorhabditis elegans. BMC Dev. Biol. *8*, 49.

Tatar, M., Bartke, A., and Antebi, A. (2003). The endocrine regulation of aging by insulin-like signals. Science *299*, 1346–1351.

Verweij, M., van Ginhoven, T.M., Mitchell, J.R., Sluiter, W., van den Engel, S., Roest, H.P., Torabi, E., Ijzermans, J.N., Hoeijmakers, J.H., and de Bruin, R.W. (2011). Preoperative fasting protects mice against hepatic ischemia/reperfusion injury: mechanisms and effects on liver regeneration. Liver Transpl. *17*, 695–704.

Villeda, S.A., Luo, J., Mosher, K.I., Zou, B., Britschgi, M., Bieri, G., Stan, T.M., Fainberg, N., Ding, Z., Eggel, A., et al. (2011). The ageing systemic milieu negatively regulates neurogenesis and cognitive function. Nature *477*, 90–94.

Wasselin, T., Zahn, S., Maho, Y.L., Dorsselaer, A.V., Raclot, T., and Bertile, F. (2014). Exacerbated oxidative stress in the fasting liver according to fuel partitioning. Proteomics *14*, 1905–1921.

Wei, M., Fabrizio, P., Hu, J., Ge, H., Cheng, C., Li, L., and Longo, V.D. (2008). Life span extension by calorie restriction depends on Rim15 and transcription factors downstream of Ras/PKA, Tor, and Sch9. PLoS Genet. *4*, e13.

Wullschleger, S., Loewith, R., and Hall, M.N. (2006). TOR signaling in growth and metabolism. Cell *124*, 471–484.

Cell Metabolism, Volume *22*

Supplemental Information

A Periodic Diet that Mimics Fasting Promotes Multi-System Regeneration, Enhanced Cognitive Performance, and Healthspan

Sebastian Brandhorst, In Young Choi, Min Wei, Chia Wei Cheng, Sargis Sedrakyan, Gerardo Navarrete, Louis Dubeau, Li Peng Yap, Ryan Park, Manlio Vinciguerra, Stefano Di Biase, Hamed Mirzaei, Mario G. Mirisola, Patra Childress, Lingyun Ji, Susan Groshen, Fabio Penna, Patrizio Odetti, Laura Perin, Peter S. Conti, Yuji Ikeno, Brian K. Kennedy, Pinchas Cohen, Todd E. Morgan, Tanya B. Dorff, Valter D. Longo

Supplementary Data

Supplementary Figures

Figure S1

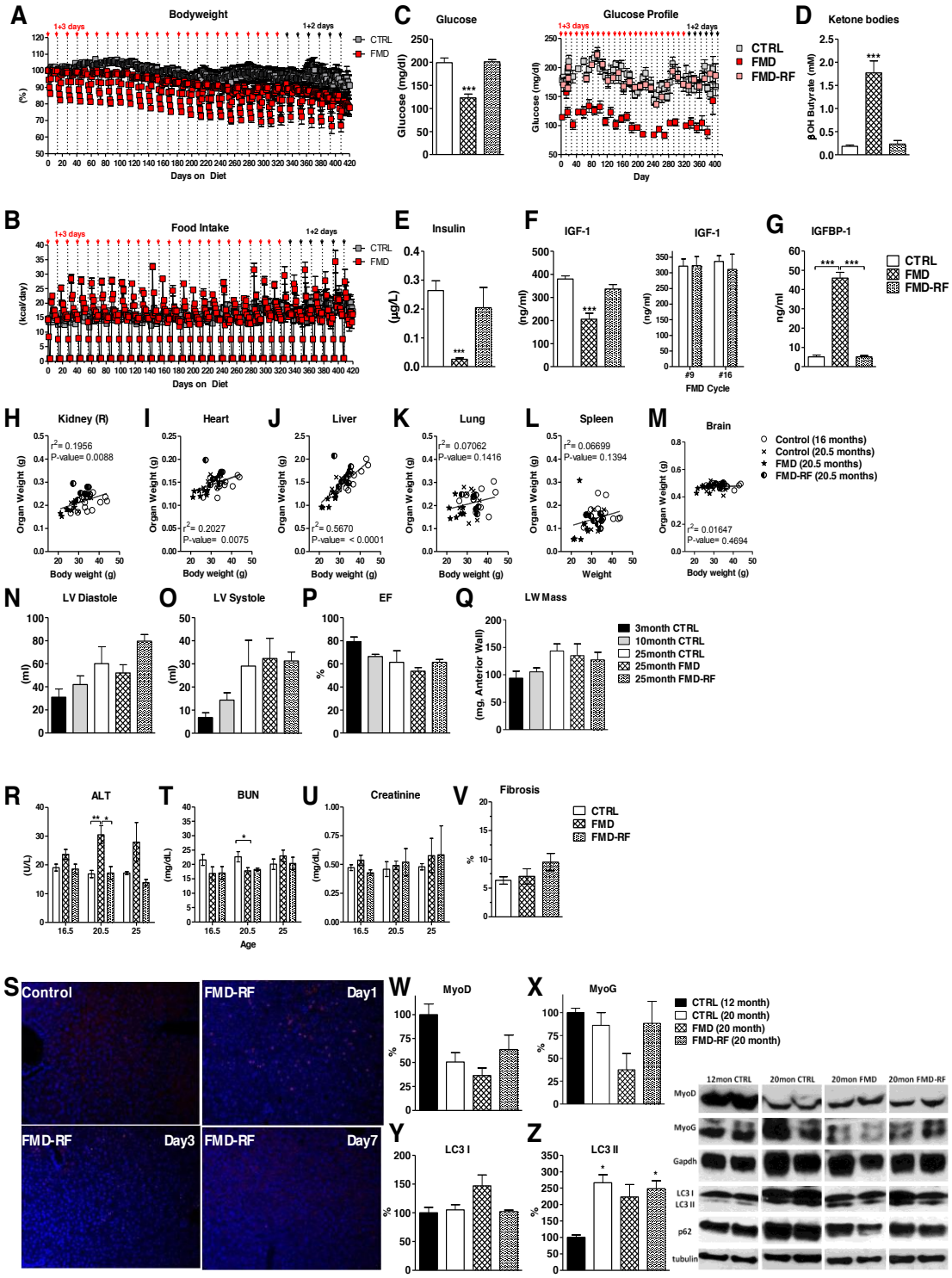

Figure S1 *(Related to Figure 1)*

A) Body weight profile in % compared to the onset of the FMD diet for the *ad lib* fed (gray) and FMD fed (red) cohort. Dashed lines and arrows indicate the onset of the bi-monthly FMD cycle. Red arrows for the 1+3 day feeding cycles, black arrows indicate the 1+2 day schedule later during the study. See text for details. n = 9/group. **B)** Food intake in kcal per day for *ad lib* (gray) and FMD (red) fed groups during the study period. Dashed lines and arrows indicate the onset of the bi-monthly FMD cycle. Red arrows for the 1+3 day feeding cycle, black arrows indicate the 1+2 day schedule later during the study. See text for details. n = 15/group. **C)** Blood glucose (in mg/dL) profile for the *ad lib* fed (gray) and FMD fed (red) cohort. Animals at the end of the FMD cycle in bright red, animals of the FMD group 7 days after re-feeding with normal rodent chow (FMD-RF) in light red. Dashed lines and arrows indicate the onset of the bi-monthly FMD cycle. Red arrows for the 1+3 day feeding cycle, black arrows indicate the 1+2 day schedule later during the study. See text for details. n = 3-5/group. **D)** Ketone bodies, **E)** Serum insulin levels and **F)** Serum insulin-like growth factor (IGF)-1 level in *ad lib* fed control animals, FMD fed and FMD-mice 7 days post re-feeding (FMD-RF) after the first cycle; as well as cycles 9 and 16 for IGF-1. n = 3-5/group. **G)** IGF binding protein-1 (IGFBP-1) measurements for *ad lib* fed control (n = 5) mice or at the end of the FMD feeding cycle (n = 5) at 17 month of age. 7 days after re-feeding, FMD animals were measured again (FMD-RF, n = 5). **H) - M)** Control fed animals were euthanized at 16 months (n = 10) prior to the start of the FMD diet to obtain baseline measurements for organ weight. Comparison of organ weight in relation to body weight for **H)** right kidney, **I)** heart, **J)** liver, **K)** lung, **L)** spleen and **M)** brain. **N)- Q)** Ultrasound echocardiogram data of young (3 months), middle-aged (10 months) and old (25 months) control fed animals as well as 25 months-old animals from the FMD cohort. FMD data obtained on the last day of the dietary regimen, FMD-

RF data 7 days post re-feeding with standard rodent chow. n = 5/group. **N)** Left ventricular (LV) volume in diastole and **O)** systole, **P)** ejection fraction (EJ), and **Q)** the (corrected) relative left ventricular wall (LW) mass were calculated. **R)** Serum alanine transaminase (ALT) level at 16.5, 20.5 and 25 months in control fed and FMD fed mice. For reference, ALT levels 7 days post re-feeding in the FMD cohort are shown (FMD-RF). All data presented as mean ± SEM; * $p<0.05$, ** $p<0.01$, ANOVA, Tukey's multiple comparison. **S)** Liver immunofluorescent staining with Ki67 (red) and DAPI (blue) in control and FMD mice at day 1, 3 and 7 post refeeding. **T)** Serum creatinine and **U)** blood urea nitrogen (BUN) level at 16.5, 20.5 and 25 months in control fed and FMD fed mice. For reference, creatinine and BUN levels 7 days after re-feeding mice in the FMD cohort with normal food are shown (FMD-RF). **V)** Quantification of Masson's trichrome stain to evaluate renal histopathology and glomerular/interstitial fibrosis in control fed mice and animals from the FMD cohort both at the end of diet and the end of re-feeding (FMD-RF). To evaluate myogenesis markers, **W)** MyoD and **X)** MyoG protein expression levels in *ad lib* fed control animals at 12 and 20 months of age in comparison to 20 months-old animal at the end of the FMD dietary cycle or one week after re-feeding (FMD-RF) with normal food were measured. Representative results shown below. n = 4/group. All data presented as mean ± SEM. Protein expression of the autophagy marker **Y)** LC3 I and **Z)** LC3 II was measured in *ad lib* fed control animals at 12 and 20 months of age in comparison to 20 months old animal at the end of the FMD dietary cycle or one week after re-feeding (FMD-RF) with normal food. Representative results shown below. n = 4/group. All data are expressed as the mean ± SEM.

Figure S2

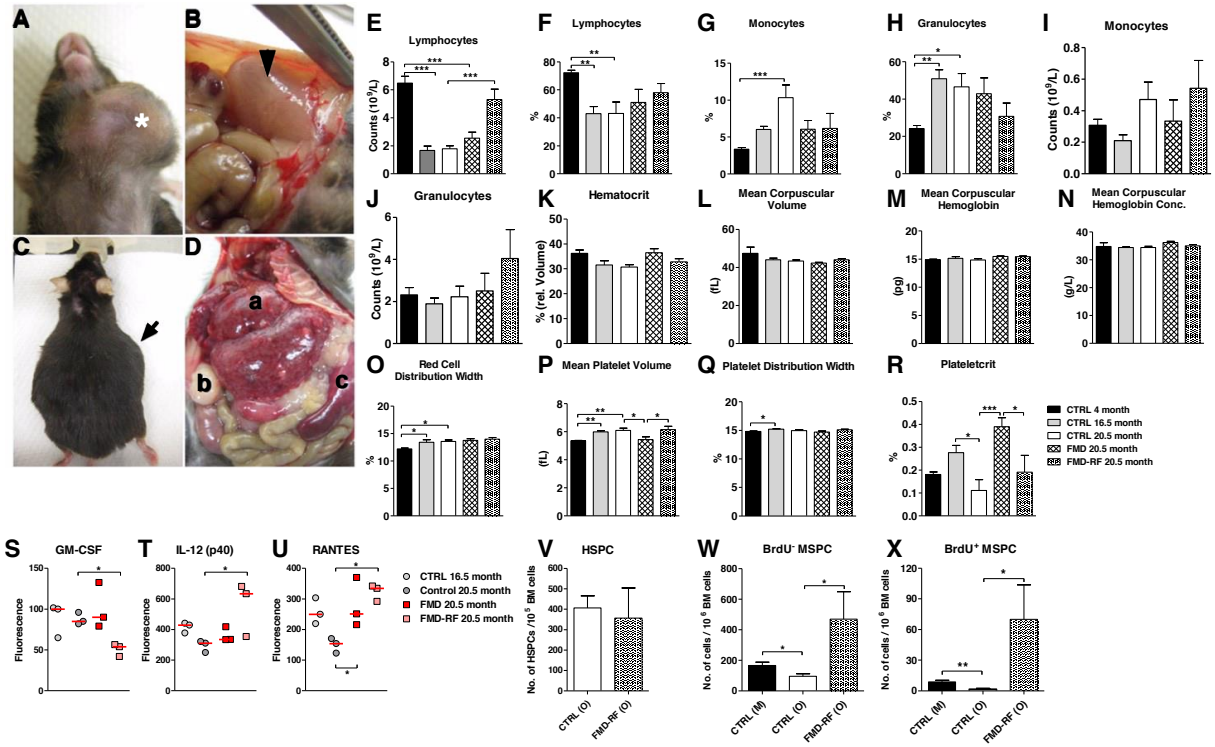

Figure S2 *(Related to Figure 2)*

A) Subcutaneous (*asterisk*) or **C)** internal masses (*arrow*) commonly found in aging animals. The appearance of these masses can be attributed to subcutaneous inflammation with resulting enlarged lymph nodes (**B**, *arrowhead*) or multi-systemic neoplasia (**D**; a: liver, b: ovaries, c: spleen)**. E)-R)** Complete blood counts (CBC) in 4 months, 16.5 months and at 20.5 months-old mice in the *ad lib* fed control and FMD cohort at the end of the FMD dietary cycle or one week after re-feeding (FMD-RF) with normal food were measured. n = 6-10/group. **S)- U)** Significantly changed cytokines out of a panel of 23 markers at age 16.5 months and 20.5 months for CTRL, FMD and FMD-refed animals. **V)** Bone marrow cells were harvested from the femur and tibia of 20.5 months-old control mice and FMD-fed mice 7 days after refeeding (FMD-RF) and stained with lineage-specific Scal-1 (PE-Cy-A) and c-Kit (APC-A) antibodies to measure hematopoietic stem and progenitor cells (HSPC). n = 6/group. All data presented as mean ± SEM. **W) - X)** To detect

the generation of stem/progenitor cells, mice were injected with bromodeoxyuridine (BrdU) 24 hours before bone marrow collection. Bone marrow cells harvested from control fed mature (M, 8-10 month) and old (O, 20.5 month) as well as 20.5 month old FMD-mice 7 days after refeeding (FMD-RF) were sorted by flow cytometry to measure pre-existing ($BrdU^-$) and newly-generated ($BrdU^+$) $Lin^-Sca1^+CD45^-$ mesenchymal stem/progenitor cells (MSPC), also known as very small embryonic like stem cells (VSEL). All data are expressed as the mean ± SEM.

Figure S3

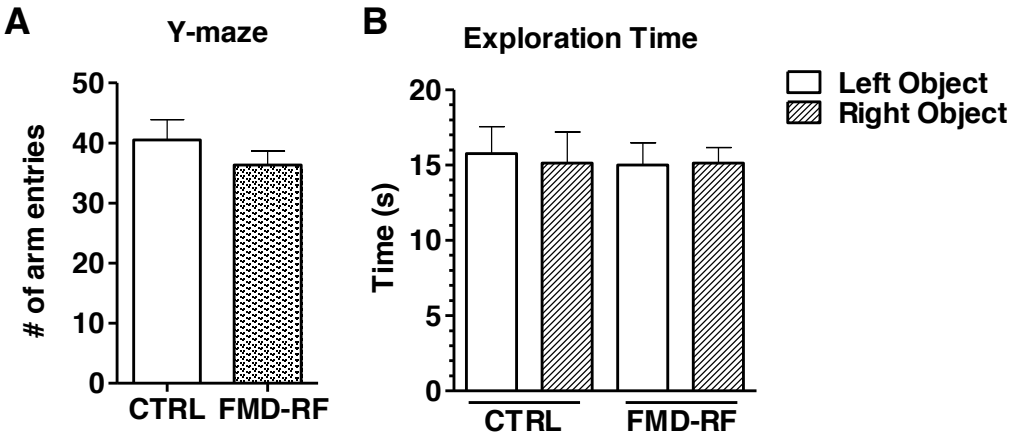

Figure S3 *(Related to Figure 3)*

A) Total number of arm entries of 23 months old (n =11) *ad lib* fed control animals and FMD-mice 7 days after refeeding (FMD-RF) in the Y-maze behavioral test. **B)** Exploration time for the two identical objects placed left and right during the adjustment phase of the novel object recognition task. n = 8/group. All data presented as mean ± SEM.

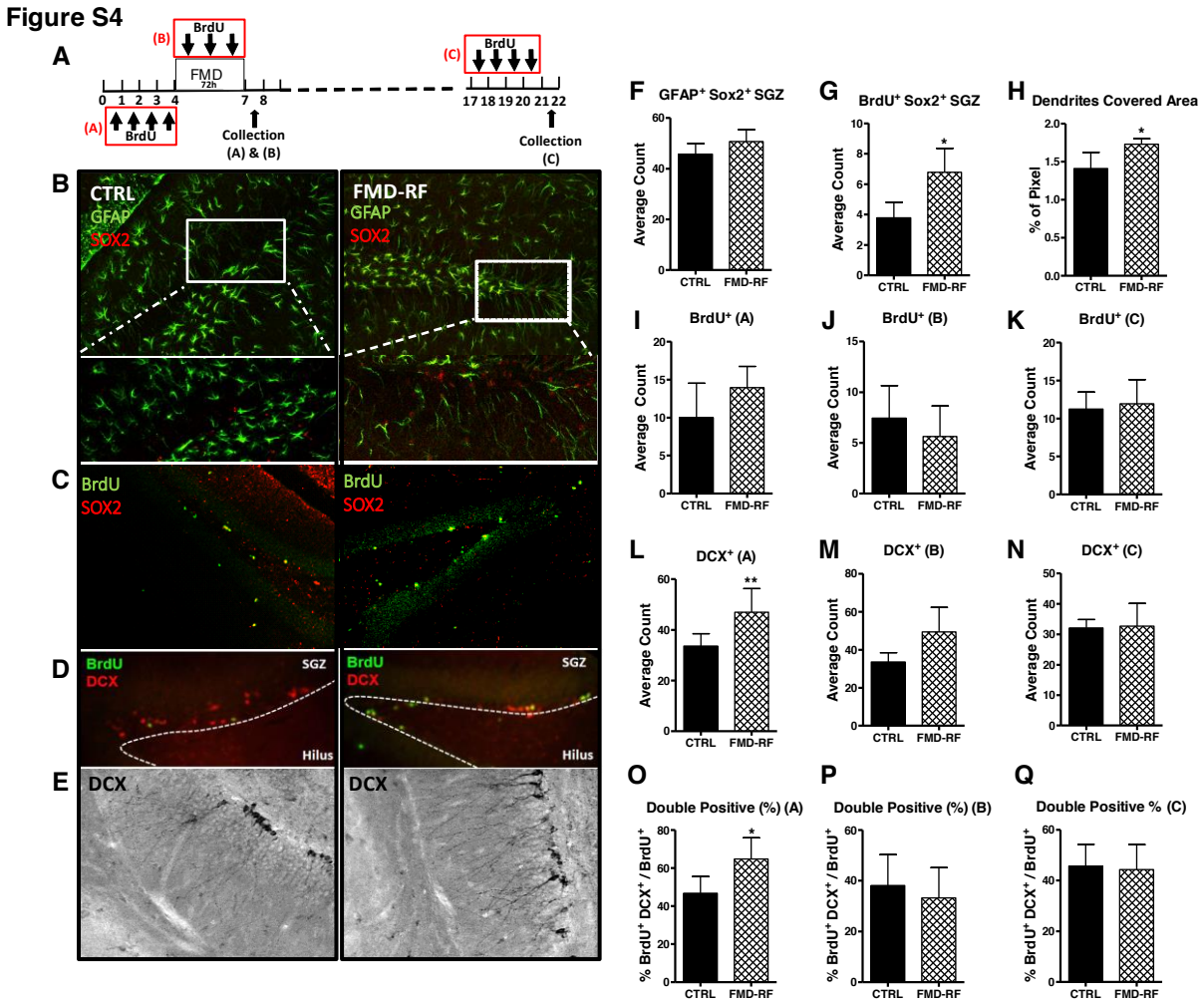

Figure S4 *(Related to Figure 4)*

A) Experimental scheme to assess neural stem cell proliferation and differentiation based on the FMD schedule (*see Methods for details*) and different BrdU injection time points in 6 months-old CD1 mice. **B)** $GFAP^+$ $Sox2^+$ (Type I neural stem cell) in the sub-granular zone (SGZ) in the control group and at the end of FMD (BrdU schedule A). **C)** $BrdU^+$ $Sox2^+$ (Type I and Type II neural stem cell) in SGZ in the control group and at the end of FMD (BrdU schedule B). **D)** $BrdU^+$ DCX^+ in SGZ in the control group and at the end of FMD (BrdU schedule A). **E)** Dendrites (DCX^+, schedule C) covered molecular layer. **F)** Quantification of $GFAP^+$ $Sox2^+$ in SGZ. **G)** $BrdU^+$ $Sox2^+$ in SGZ,

increased BrdU incorporation in $Sox2^+$ cells indicating self-renewal/proliferation of neural stem cell in the FMD cohort (n = 4/group). **H)** Quantification of dendritic covered area of the molecular layer 3 weeks after FMD. **I-Q)** Quantification of $BrdU^+$ (I- H), DCX^+ (L- N) and double positive for $BrdU^+$ DCX^+ over $BrdU^+$ cells (O- Q) at time points A, B and C. All data are expressed as the mean ± SEM.

Figure S5

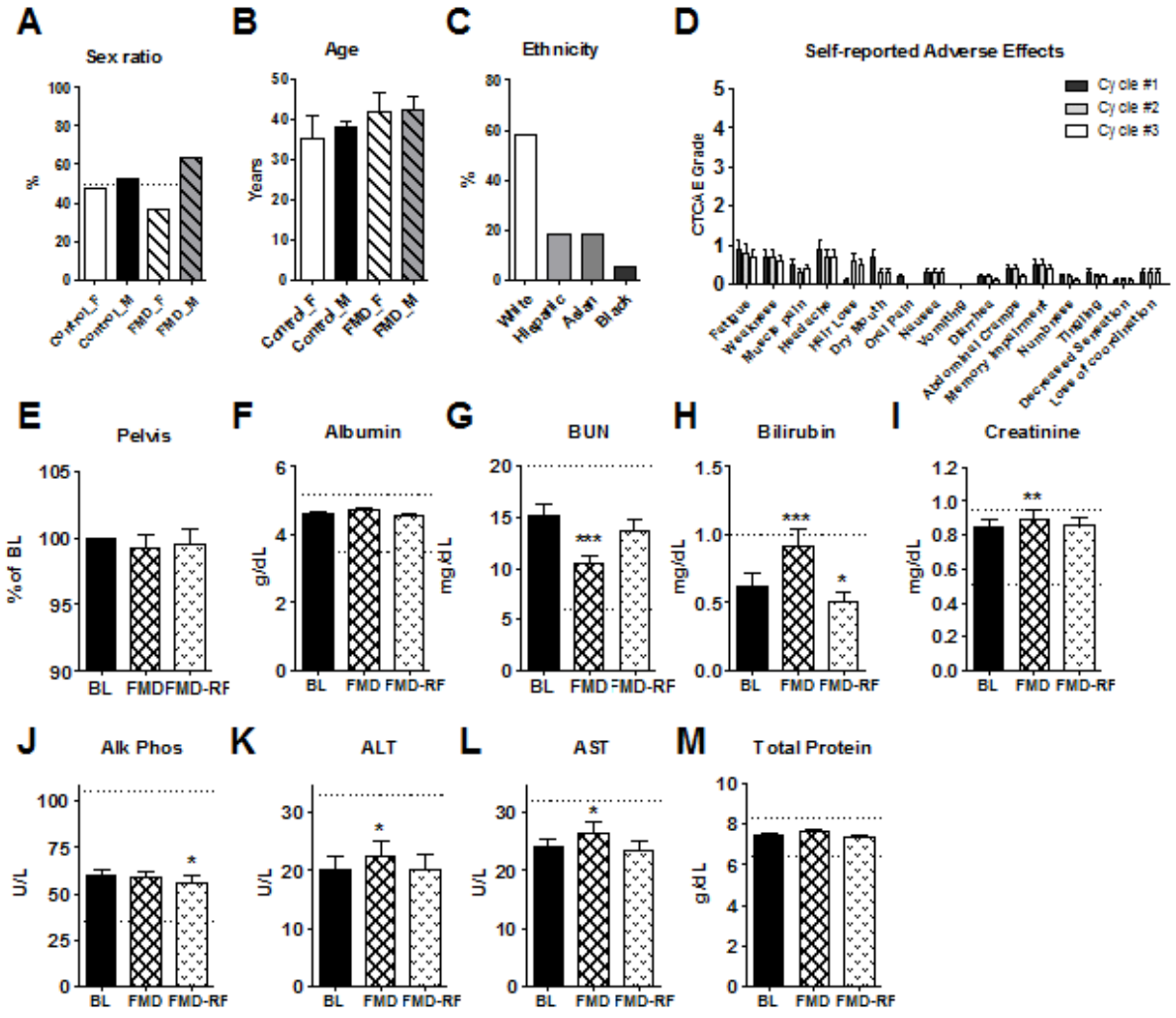

Figure S5 *(Related to Figure 6)*

A) Percentage of female (F) and male (M) participants in the control or FMD groups that were part of a randomized clinical study to evaluate the human FMD version. **B)** Gender specific average age per group. **C)** Ethnic background. **D)** Subject self-reported adverse effects based on Common Terminology Criteria for Adverse Effects (CTCAE; 1 = Mild, 2 = Moderate, 3 = Severe, 4 = Life-threatening, 5 = Death). **E)** Bone mineral density (BMD in g/cm^2; n = 19) was evaluated by dual-energy X-ray absorptiometry and compared to control. Safety and feasibility were evaluated based on complete metabolic panels (**F- M**; n = 19) prior to (Baseline, BL), during (FMD) and after completion of 3 FMD cycles (FMD-RF). All data are expressed as the mean ± SEM.

Table S1 Fasting and the Fasting Mimicking Diet (FMD) induce a similar physiological response in mice. *(Related to Figure 1)*

	Fasting (72 hours)			**FMD (96 hours)**	
	Effect	*Change*	*Reference*	*Effect*	*Change*
Blood glucose	↓	~45%	(Lee et al., 2010; Wang et al., 2006)	↓	~40%
Ketone bodies	↑	~10-fold *	(Shimazu et al., 2013)	↑	~10-fold
IGF-I	↓	~40- 70%	(Brandhorst et al., 2013; Frystyk et al., 1999; Lee et al., 2010)	↓	~45%
IGFBP-1	↑	~7- 11-fold	(Frystyk et al., 1999; Lee et al., 2010)	↑	~8-fold

* after 24 hours of fasting. *Abbreviations*: IGF-I, insulin-like growth factor 1; IGFBP-1, insulin-like growth factor binding protein 1.

Table S2 Overview of autopsy results from the *ad lib* control and Fasting Mimicking Diet (FMD) mouse cohorts. *(Related to Figure 2)*

	Ad lib		FMD	
	Total	%	Total	%
Lymphoma	30	66.7	11	39.3
Liver	11	24.4	4	14.3
Lymphocytic infiltration	1	2.2		
Fibrosis	1	2.2	1	3.6
*Necrosis (*with Inflammation)*	2	4.4	1	3.6
Infarct	1	2.2	1	3.6
Congested	3	6.7	1	3.6
Chronic inflammation	2	4.4		
(Diffuse) Acute inflammation	1	2.2		
Spleen	3	6.7	3	10.7
Organized thrombus			1	3.6
Infarct	2	4.4	1	3.6
Extensive medullary hematopoiesis	1	2.2		
*Follicular hyperplasia^*			1	3.6
Kidney	1	2.2	1	3.6
Cortical cysts			1	3.6
Medullary cyst	1	2.2		
Ovary/ Ovaduct	5	11.1	1	3.6
Hemorrhagic cyst	1	2.2		
*Necrosis**			1	3.6
Fibrosis	1	2.2		
Dilated fluid-filled uterine horn	1	2.2		
Calcification	1	2.2		
Cyst attached to uterine horn (benign)	1	2.2		
Urinary bladder	0	0.0	1	3.6
Dilated, edematous			1	3.6
Lungs	1	2.2	2	7.1
Aspiration pneumonia			2	7.1
Atypical/mitotically active infiltrate#	1	2.2		
Pancreas	0	0.0	1	3.6
Granuloma			1	3.6
Lymphnodes	2	4.4	0	0.0
Reactive	1	2.2		
Cavernous hemangioma†	1	2.2		
Others	6	13.3	0	0.0
Myositis	1	2.2		
Cutaneous hemangioma	1	2.2		
Fibrosarcoma (subcutan)	2	4.4		
Enlarged salivary gland	2	4.4		

Total incidence and percentage is shown per organ (gray rows) and individual abnormality. Lymphoma incidence involves both systemic and localized cases. ^, consistent with chronic inflammation; *, possibly due to torsion; #, consistent with lymphoma; †, associated with chronic inflammation with numerous plasma cells and reactive mast cells.

Table S3 Complete blood counts of young and 20.5 months-old mice. *(Related to Figure 2)*

	4 Month	20.5 month					
	CTRL	**CTRL**		**FMD**		**FMD-RF**	
White Blood Cell count (10^9/L)	9.13 ± 0.85	4.49 ± 0.59	^	5.38 ± 0.92		9.90 ± 2.04	†
Lymphocyte count (10^9/L)	6.48 ± 0.49	1.79 ± 0.22	^^^	2.55 ± 0.43	‡‡	5.31 ± 0.73	†††
Monocyte count (10^9/L)	0.31 ± 0.04	0.47 ± 0.11		0.33 ± 0.14		0.54 ± 0.18	
Granulocyte count (10^9/L)	2.32 ± 0.34	2.23 ± 0.50		2.50 ± 0.84		4.04 ± 1.37	
Lymphocyte (%)	72.29 ± 1.74	43.09 ± 8.26	^^	51.07 ± 9.27		57.94 ± 6.61	
Monocyte (%)	3.34 ± 0.22	10.34 ± 1.70	^^^	6.05 ± 1.18		6.19 ± 2.01	
Granulocyte (%)	24.20 ± 1.60	46.57 ± 7.14	^	42.88 ± 8.49		30.76 ± 7.11	
Red Blood Cell count (10^9/L)	8.59 ± 0.19	7.10 ± 0.22	^^	8.64 ± 0.34	**,‡	7.47 ± 0.32	
Hemoglobin (g/L)	12.88 ± 0.27	10.57 ± 0.30	^^	13.42 ± 0.57	**,‡	11.57 ± 0.54	
Hematocrit (rel. volume of erythrocytes)	36.23 ± 1.35	30.70 ± 0.94		36.50 ± 1.62	*	32.86 ± 1.24	
Mean Corpuscular Volume (fL)	47.42 ± 3.32	43.36 ± 0.62		42.30 ± 0.38		44.10 ± 0.54	
Mean Corpuscular Hemoglobin (pg)	14.94 ± 0.05	14.86 ± 0.23		15.47 ± 0.09		15.44 ± 0.12	
Mean Corpuscular Hemoglobin Concentration (g/L)	34.84 ± 1.34	34.41 ± 0.49		36.22 ± 0.46	*	35.10 ± 0.39	
Red Cell Distribution Width	12.23 ± 0.13	13.57 ± 0.28	^	13.75 ± 0.31		13.99 ± 0.32	
Platelet Count (10^9/L)	348.40 ± 13.38	192.90 ± 82.75		712.80 ± 53.82	**,‡	325.00 ± 124.00	
Mean Platelet Volume (fL)	5.38 ± 0.0.	6.10 ± 0.16	^^	5.45 ± 0.19		6.16 ± 0.24	
Platelet Distribution Width	14.83 ± 0.05	14.97 ± 0.12		14.70 ± 0.19		15.10 ± 0.12	
Plateletcrit	0.18 ± 0.01	0.11 ± 0.05		0.39 ± 0.034	**	0.19 ± 0.07	

^ p< 0.05, ^^ p<0.01, ^^^ p<0.001 young (4 months) compared to old (20.5 months); * p< 0.05, ** p<0.01, *** p<0.001 young (4 months) compared to old (20.5 months); † p< 0.05, †† p<0.01, ††† p<0.001 young (4 months) compared to old (20.5 months); ‡ p< 0.05, ‡‡ p<0.01, ‡‡‡ p<0.001 young (4 months) compared to old (20.5 months).

Table S4 Caloric content of the human FMD regimen. *(Related to Figure 6)*

	Day 1	Day 2- 5
Calories	~1090	~725
Protein (%)	10	9
Fat (%)	56	44
Carbohydrates (%)	34	47

Supplemental Experimental Procedures:

Physiological Biomarkers β–hydroxybutyrate was measured with a colorimetric assay kit following the manufacturer's protocol (#700190, Cayman Chemical). Insulin level were measured using a mouse/rat specific ELISA (Millipore, #EZRMI-13K) following the manufacturer's protocol. Human serum IGF-I and IGFBP-1 was measured with an in-house enzyme-linked immunosorbent assay (ELISA) based on paired specific antibodies (R&D Systems) and validated against the commercial kit from Diagnostic Systems Laboratories. CRP levels were measured with a human specific ELISA kit following the manufacturer's protocol (R&D Systems, #DCRP00). Mouse serum IGF-I was measured using a mouse specific ELISA kit (R&D Systems). Mouse serum IGFBP-1 levels were measured by in-house ELISA assays using recombinant mouse proteins and antibodies from R&D Systems (MAB 1240 as capture antibody and BAF 1240 as detection antibody, R&D Systems, Minneapolis, MN, USA) as described previously (Gray et al., 2011). PKA activity was measured using ENZO PKA kinase activity kit (ENZO Lifesciences ADI-EKS-390A). Mouse kidney function was evaluated by serum creatinine and blood urea nitrogen (BUN) at 16.5, 22 and 27 months of age based on a quantitative colorimetric assay (Quantichrome^{TM}; DICT-500 and DIUR-500, respectively) following the manufacturer's protocol (BioAssay Systems). In brief, 30 µl serum (for creatinine) or 5 µl (for BUN) and 200 µl working solution were added into a 96 well plate. Mouse liver function was analyzed by measuring serum alanine transaminase (EnzyChrom^{TM}; EALT-100) following the manufacturer's protocol (BioAssay Systems). In brief, 20 µl serum and 200 µl working solution were added into a 96 well plate.

X-ray computed tomography (CT)-Scans *(continued)* CT phantoms for density calibration were used to fit data and determine the slope and intercept. Images were reconstructed and densities calculated based on the phantom scan values. The slope and intercept of the phantoms were used to interpolate/extrapolate the tissue mineral density (TMD) for the femur of all animals. The reported tissue mineral density of the investigated bone volume contains hydroxyapatite contribution from both the cortical and trabecular bone.

The body fat composition was measured *in vivo* for N=3/group. The abdominal region of each mouse was scanned with a Siemens InveonCT scanner at the following settings: 80 kV, 250 μA, 220° total rotation in 180 rotation steps, binning of 4 and 300 ms exposure time. Two-dimensional gray-scale image slices were reconstructed into a three-dimensional tomography. Scans were reconstructed between the proximal end of L1 and the distal end of L5 using COBRA software. The region of interest for each animal was defined based on skeletal landmarks from gray-scale images. To analyze total fat volume, a threshold segmenting fat from other tissues and background was determined by *ex vivo* microCT imaging of a freshly harvested fat pad, muscle and liver tissue from a C57BL/6J mouse. The abdominal muscular wall was used as the demarcation line to separate visceral adipose tissue from subcutaneous adipose tissue. Fat scans by means of microCT were performed 5 days following refeeding to avoid interferences during the immediate recovery time from the FMD.

Immunohistochemistry Adult mice were anesthetized with isoflurane and intracardially perfused with saline followed by 4% paraformaldehyde (PFA). The tissues were removed immediately and post-fixed in 4% PFA for 24 hours and stored in 0.05% sodium azide. Brain was cut sagittally (40 μm), and stored in 0.05% sodium azide solution. Briefly, the sections were rinsed 3 times in

phosphate buffered saline (PBS) for 5 minutes and denatured in 2N HCl at 37°C for 20 minutes. Sections were neutralized with 0.1M boric acid for 10 minutes and blocked with 2% Normal Donkey Serum (NDS; Jackson ImmunoResearch) for 1 hour at room temperature. For liver, samples were obtained from the right lobe and processed for paraffin embedding and sectioning at the USC Stem Cell Core. Hepatic proliferation was assessed by Ki67 (Santa Cruz) staining on days 1, 3 and 7 post refeeding following the BrdU protocol. For the evaluation of adult neurogenesis in the hippocampus, sections were incubated in BrdU (Serotec, 1:200), doublecortin (Santa Cruz, 1:200), GFAP (Cell Signaling, 1:200), Sox2 (Millipore, 1:100), diluted in 2% NDS in 0.3% triton overnight at 4°C. The sections were rinsed 3 times in PBS for 10 min, incubated in anti-rat IgG tagged with Alexa Flour488 and anti-goat IgG tagged with Alexa Flour598 (Invitrogen, 1:400) diluted in 2% NDS. Sections are mounted using Vectashield (Vector). Free-floating hippocampal (one out of every 6^{th}) were processed for fluorescent immunohistochemistry. Co-expression was confirmed by fluorescent- and confocal-microscopy. Ki67-positive cells were quantified by averaging at least 5 consecutive, non-overlapping image frames from at least two tissue sections 30 μm apart. Digital images were collected on a Leica SL confocal microscope located at the Multiphoton Imaging Core of the University of Southern California. For quantification, serological counting methods were used.

Western blotting *(continued)* About 50 mg of muscle (*m. gastrocnemius*) was homogenized in 80 mM Tris-HCl, pH 6.8, containing 100 mM DTT, 70 mM SDS, and 1 mM glycerol, with freshly added protease and phosphatase inhibitor cocktails, kept on ice for 30 min, centrifuged at 15000 x g for 10 min at 4°C, and the supernatant was collected. Protein concentration was assayed using BSA as working standard. Equal amounts of protein (30 μg) were heat-denaturized in sample-

loading buffer (50 mM Tris-HCl, pH 6.8, 100 mM DTT, 2% SDS, 0.1% bromophenol blue, 10% glycerol), resolved by SDS-PAGE and transferred to nitrocellulose membranes (Bio-Rad, Hercules, CA, USA). The filters were blocked with Tris-buffered saline (TBS) containing 0.05% Tween and 5% non-fat dry milk and then incubated overnight with antibodies directed against MyoD, and myogenin (Santa Cruz Biotechnology, CA, USA), the monoclonal antibody against Pax7 (developed by Atsushi Kawakami, obtained from the Developmental Studies Hybridoma Bank (University of Iowa)) and LC3B (L7583; BD Biosciences, San Jose, CA). Peroxidase-conjugated IgG (Bio-Rad, Hercules, CA, USA) was used as secondary antibody. Membrane-bound immune complexes were detected by an enhanced chemiluminescence system (Santa Cruz Biotechnology, USA) on a photon-sensitive film (Hyperfilm ECL, GE Healthcare, Milano, Italy). Protein loading was normalized according to tubulin or GAPDH expression. Quantification was performed by densitometric analysis using TotalLab software (NonLinear Dynamics, Newcastle upon Tyne, UK).

Quantitative PCR Relative transcript expression levels were measured using a SYBR Green-based method. IGF1R F-CAAGCTGTGTGTCTCCGAAA/R-CTCCGTTGTTCCTGGTGTTT and NeuroD1 F-ATTGCGTTGCCTTAGCACTT/R-TGCATTTCGGTTTTCATCCT. Average fold changes were calculated by differences in threshold cycles (Ct) between pairs of samples.

Behavior Studies *(continued)* To prevent starvation-induced hyper-activity (e.g. foraging associated movement (personal observation SB)), FMD animals were exposed to the behavior tests not earlier than 3 days after re-feeding. Y-maze Short-term spatial recognition memory was examined by a spatial novelty preference task in the Y- maze. The Y- maze was made of black

plexiglas and comprised three identical arms (50 × 9 × 10 cm), radiating from a central triangle (8 cm on each side) and spaced 120° apart from each other. The test started placing the rodent in one of the arms of the maze. The mouse was allowed to freely explore the environment for 8 minutes and the total numbers of arm entries and arm choices were recorded. Arm choices are defined as both fore-paws and hind-paws fully entering the arm. We used an Accelerating rotarod consisting of a 3 cm diameter rotating rod (suspended 15 cm above the base) and divided by flanges so that up to 5 mice could be tested simultaneously. Mice were placed on the rotating rod and the speed gradually increased from 4 rpm to 40 rpm within a 5 min session. The exact speed at which the mice fell off and time that the mice were able to stay on the bar were recorded. On two consecutive days, the mice were given three successive trials, for a total of six trials. Novel Object Recognition The novel object recognition test was introduced to assess the ability of rodents to recognize a novel object in a familiar environment. The test includes a habituation phase (5 min on day one) and trial phases (5 min each on the second day) for each mouse. Briefly, in the habituation phase, the mouse was placed into a rectangular cage (50 x 50 x 40 cm) made of black acryl plexiglas for 5 min on day one without any object. The testing session comprised two trials with the duration of each trial being 5 min. Mice were always placed in the apparatus facing the wall at the middle of the front segment. Exploration of the objects is defined as any physical contact with an object (whisking, sniffing, rearing on or touching the object) as well as positioning its nose toward the object at a distance of less than 2 cm; however, sitting or standing on top of the object is not counted toward the exploration time. After the first exploration period, the mice were placed back in their home cage. To control for odor cues, the open field arena and the objects were thoroughly cleaned with water, dried, and ventilated for a few minutes between mice. After a 1 hour delay interval, mice were placed back in the apparatus for the second trial (T2), but now with two

dissimilar objects, a familiar one and a new one. Barnes Maze The maze consists of a platform with 20 holes (San Diego Instruments) and 20 boxes underneath each hole; with only one hole big enough to allow the entire mouse to enter/hide (escape box, ”EB”). A unique position for the EB was randomly assigned to each mouse; this position was always located underneath the same hole for a specific animal. In order to minimize the inter-maze cues, the platform was rotated after each trial. All mice were trained once daily on days 0 to 7. During training sessions, mice were allowed to freely explore the maze until either entering the EB or after 2 min time elapsed. If the mouse did not enter the EB by itself, it was gently guided to and allowed to stay in the EB for 30 seconds. After the training session, mice were tested twice daily for 7 days. Testing was similar to training, but if after 2 min the mouse did not find the EB, it was directly returned to its cage.